CERN/DRDC/90-38
DRDC/P8
29th August 1990

DETECTOR R&D PROPOSAL

INTEGRATED HIGH-RATE TRANSITION RADIATION DETECTOR AND TRACKING CHAMBER FOR THE LHC

V.A. Polychronakos
Brookhaven National Laboratory, USA

H. Beker, R.K. Bock, E. David, C.W. Fabjan*, J. Pfennig,
M.J. Price and W. J. Willis
CERN, Geneva, Switzerland

Y. Ershow, I. Golutvin, N. Gorbunov, V. Karzhavin,S. Khabarov,
V. Khabarov, A. Liubin, V. Peshekonov and D. Smolin
JINR (Dubna), USSR

T. Akesson
University of Lund, Sweden

V. Chernyatin, B. Dolgoshein**, A. Konstantinov, P.Nevski,
M. Potekhin, A. Romaniouk, S. Smirnov and V. Sosnovtsev
Moscow Physical Engineering Institute, Moscow, USSR

I. Gavrilenko, S. Maiburov, S. Muraviev and A. Shmeleva
P.N. Lebedev Institute of Physics, Moscow, USSR

SUMMARY

The development of an integrated transition radiation detector (TRD) and charged-particle tracker for use in an LHC detector is proposed. The purpose of such a detector is to identify electrons efficiently, while rejecting the potentially very large background, originating mainly from overlaps between an energetic π^0 and a charged hadron and from electron pairs. A low-mass structure of radiator materials and proportional straws will generate and detect transition radiation X-rays and will track charged particles. Readout for the straw signals, and trigger processors correlating the TRD signal with external detectors, will be developed. A small prototype, sufficient to contain a high-energy jet and followed by a fine-grained calorimeter, will be tested. An engineering prototype will be constructed to verify the design for a large detector.

* Contact person
** Spokesperson

1. INTRODUCTION

It is beyond the scope of this proposal to examine in detail the physics goals of the LHC, which is expected to operate at a centre-of-mass energy of 16 TeV and at luminosities exceeding 10^{34} cm^{-2} s^{-1} [1]. Because of the very large QCD jet cross-sections predicted at LHC energies, the most accessible signature for new massive particles is expected to be obtained through the study of leptonic channels comprising one or more high-energy electrons and/or muons in the final state. Efficient identification of electrons and muons, over a large solid angle and down to transverse momenta of 10 to 20 GeV, is required in order to achieve sufficient acceptance for some of these low-rate multileptonic decays.

The main goal of this proposal is to tackle the difficult problem of electron identification, beyond the level of electromagnetic calorimetry. Transition radiation is potentially a powerful tool for particle identification [2], and its measurement is complementary to calorimetric measurements since the radiation process does not affect the particle energy and direction significantly. The practical theory of transition radiation is well understood [3], and reliable calculations can be made for the design and optimization of a transition radiation detector (TRD). Many such detectors have been proposed, built, and used successfully in accelerator experiments, even at hadron colliders [4-14]. Several studies have considered the inclusion of TRDs in the LHC and SSC detectors [15-16].

We find that adequate performance of a TRD system requires a thickness which depends on operating luminosity. At this number is ~ 50 and ~ 70 cm at low respective high luminosity [15,17]. The same space may be also needed for part of the tracking system, if tracking and transition radiation detection cannot be combined in one single detector. We propose to optimize the system performance by combining these two functions in an integrated TRD and charged-particle tracker. Proportional straw chambers filled with a xenon-enriched gas will detect X-rays from transition radiation as well as the ionization from charged particles. The radiator material will provide mechanical support and rigidity for the straws. This approach has the advantages of very high rate capability, modular construction, and reliable performance.

Experiments at the LHC will require the use of as much information in real time as possible, in order to achieve the large reduction factor that is necessary between the raw event rate of up to 10^8/s and the number of events that can reasonably be expected to be recorded for later study. Active devices capable of reducing raw data to physically meaningful quantities will be needed. It is our intention to study and develop the readout architecture for the TRD-tracker so that it will contribute to the formation of a refined

electron trigger. Another important component used in obtaining a selective electron trigger is an electromagnetic and hadronic calorimeter of adequate granularity. For the development phase of this R&D programme, we propose to adapt the NA34 uranium/liquid-argon calorimeter, which will then be used as a first LHC calorimeter prototype in an electron-trigger hardware chain.

The main goals of this Proposal are:

- detailed Monte Carlo studies of the performance of the proposed system in a realistic LHC environment for luminosities in excess of 10^{34} cm^{-2} s^{-1};
- studies of mechanical support, gas manifolding, heat flow, and signal routing;
- detailed studies of proportional straw performance, including pulse shapes and drift times in various gases, radiation tolerance, and X-ray response;
- development and characterization of various materials for the radiators;
- emphasis on the development of a readout architecture, consistent with the trigger requirement and the desired performance of the detector (e.g. low-mass signal connections);
- an exploratory project to implement, in the electronics and in the readout system, the algorithms allowing optimal use of the TRD and tracking information on a time-scale suitable for event triggering, using massively parallel and/or pipelined processors;
- three stages of construction and testing of prototypes:
  1) a 180-straw detector for single particles in a test beam. First, preliminary, results obtained in June–July 1990 are presented in a subsequent section;
  2) a 1200-straw detector for studies of jets produced by 450 GeV protons;
  3) an engineering prototype representing the smallest symmetry element of the final detector, with about 15,000 straws, integrated electronics, and tested in a realistic environment with a detector system including a segmented pad chamber and a finely segmented calorimeter.

The project is expected to require four years — two for the R&D stage and two for the engineering of prototypes. At the end of this time we will have fully developed the designs and technology for such an LHC detector system, and have tested a large engineering-prototype detector in order to verify the approach. Milestones for the project are presented later in this document.

2. ROLE OF A TRD-TRACKER

The main role of a TRD-tracker is to provide rejection against fake electrons, which arise from pathological jet fragmentation and which can simulate an isolated electromagnetic shower in the calorimeter, matched to a reconstructed charged track. At the very high

luminosities considered here, the pile-up of energy from the many simultaneous interactions within even the same bunch crossing, will limit the precision on the electromagnetic shower position, from the calorimeter measurements, to approximately σ = 5 mm [18].

We therefore consider the TRD-tracker as a device which must eliminate the background from fake electrons, defined as reconstructed charged tracks pointing to within ±2 cm from an isolated electromagnetic shower, measured in the calorimeter at a radius r = 130 cm. The dominant contributions to this background are:

a) overlaps of an energetic photon from meson decays and a charged particle from a QCD jet;
b) energetic charged hadrons that shower early in the electromagnetic calorimeter;
c) electron pairs arising from π^0 and η Dalitz decays;
d) accidental overlap of a prompt energetic photon with a charged hadron from the spectator particles (underlying event);

These backgrounds have been simulated using the ISAJET Monte Carlo program [19]. Backgrounds (a) to (c) were simulated using inclusive jets of transverse momentum p_T, larger than 25 GeV. The cross-section for this process is ~ 250 μb, for jet pseudorapidities between - 1.5 and + 1.5. In addition to the final-state particles from the QCD hard scattering process itself, an average of 50 minimum-bias events (each tuned to yield ~ 6 charged particles per pseudorapidity unit) were superimposed in order to simulate the expected particle multiplicities at the LHC for a luminosity of 2 x 10^{34} cm^{-2} s^{-1} and an integration time of 30 ns, corresponding to the drift time in the proposed straw detector.

Fig.1 shows the expected rates, for p_T > 25 and 50 GeV, for backgrounds (a) and (b), which corresponds to a small fraction (approximately ~ 0.4%) of the generated jets. The only jets that are kept are those that yield an electromagnetic transverse energy larger than 25 GeV in a (4 × 4) cm^2 cell, situated at a radius r = 130 cm, and for which at least one charged-hadron track matches the shower centroid within 2 cm. These background rates are plotted as a function of ΔR, the size of the isolation cone in azimuth-pseudorapidity space, $\Delta R = (\sqrt{\Delta\phi^2 + \Delta\eta^2})^{1/2}$: the only jets that are are kept, are those for which the total energy deposited in this cone (minus the electromagnetic energy in the trigger cell) is less than 10 GeV. This isolation cut (which includes, to some extent, a cut on the hadronic leakage behind the trigger cell) reduces the background from sources (a) and (b) by more than one order of magnitude. For ΔR > 0.2, about half of the expected background arises from accidental overlap between an isolated π^0 and a charged track from the 50 superimposed minimum-bias interactions. The uncertainties in these background rates come mainly from the jet cross-section and the jet fragmentation, especially for large

values of ΔR; the total uncertainty in backgrounds (a) plus (b) should be at least a factor 2 to 3. Within the uncertainties of the simulation, background (a) is much larger than (b), even for $\Delta R > 0.2$.

Background (c) is shown as a dashed curve in Fig. 1, and was obtained from the inclusive π^0 spectrum by scaling it down by the 1.2% branching ratio for π^0 Dalitz decay. This background is only ~ 10 times smaller in rate than the solid curve, and can easily be scaled to include inevitable conversions in the beam pipe and in the detector material in front of the calorimeter.

The production cross-section for direct photons with $p_T > 25$ GeV is ~ 75 nb. Background (d) is also shown in Fig. 1; it corresponds to the accidental overlap between a direct photon and a charged hadron. The shape of this curve as a function of the isolation cut is therefore the same as that expected for isolated electrons from $W \rightarrow e\nu$ or $H \rightarrow WW \rightarrow e + X$ decays, as can be seen in Fig. 1.

Finally, Fig. 1 shows for completeness and for comparison with the most abundant sources of prompt electrons –in addition to the expected rate for $W \rightarrow e\nu$ decays– the sources of electrons from heavy-flavour semi leptonic decays ($c,b \rightarrow e + X$) and top-quark decays ($t \rightarrow e + X$, $m_t = 130$ GeV). As expected, the electrons from c,b decay are not isolated and their rate is expected to be reduced by a factor of ~ 50 with an isolation cut at $\Delta R \approx 0.2$. Unfortunately, the expected rates for electrons from c,b decay are at present uncertain to within a factor of at least 5, and should therefore be treated with some caution [20].

Several general remarks should be made regarding Fig. 1:

i) A reasonable goal for a TRD system would be to reject all backgrounds from (a) to (d) to a level where prompt electrons from c,b and W decay become the dominant contribution to the rates shown in Fig. 1a, which would mean a rejection of ~ 100 against charged hadrons and electron pairs, including those produced in the TRD system itself.

ii) A more precise matching of the charged track to the electromagnetic shower would of course greatly reduce backgrounds (a), (b) and (d). For example, a matching requirement of better than 2 mm would reduce their rates by approximately a factor of 100, thus leaving background c) from electron pairs as the dominant one by far.

iii) Figure 1 is valid only in the absence of a central magnetic field. As will be discussed in the following, the performance of the proposed TRD system is, in a first approximation, not very different in the presence of a weak magnetic

field. With the same approach, we propose to study the relative contributions of backgrounds (a) to (d), in a weak magnetic field, with particular attention being given to the irreducible contribution from asymmetric Dalitz decays or conversions.

iv) For a higher electron threshold, p_T > 50 GeV, the acceptance for Higgs is reduced by approximately 30%. The fake−electron rate is, however, reduced by a factor of 10 to 100, depending on the isolation requirement. Nevertheless, fake electrons remain the dominant background.

From the Monte Carlo studies summarized in Fig. 1, we conclude that inclusive electron identification at the LHC cannot be achieved with calorimetry and tracking alone, but requires additional electron identification criteria. In the following, we will show, with the proposed TRD system, how we expect to achieve a rejection of ~ 100, in addition to the calorimetry and tracking, against the backgrounds studied in this section.

3. THE CONCEPTUAL DESIGNS OF THE TRD−TRACKER

One basic approach to achieving optimum electron/pion discrimination is the use of many, rather thin radiators, and correspondingly frequent measurements of the TR photons [15]. The application of this concept to collider detectors has already been discussed [16−17]. We prefer to use individual detection elements, i.e. STRAWS, embedded in the radiator, as shown conceptually in Fig. 2.

We have evaluated a number of detector geometries, resulting in two concepts, shown in Figs. 3 and 4, which have the following characteristics:

i) all straws are oriented in a plane perpendicular to the beam; they provide tracking in the r−z plane and detection of the TR X−rays;

ii) the straws are relatively short, in the range 35 to 100 cm, and subtend a fixed pseudorapidity interval, independent of z, and hence have an η−independent occupancy;

iii) the azimuthal straw array gives good pointing to the beam line for track association with the correct primary vertex;

iv) layer−to−layer occupancy correlations, due to particles from different interactions separated by more than a few millimetres along the beam line, are reduced;

v) the effective length of the TRD depends on the polar angle as $(\sin\theta)^{-1}$. It provides an e/π discrimination that is approximately constant for particles with a given p_T, independent of θ;

vi) even in the case of a weak axial magnetic field, the electrons from a conversion will not be measured in different straws, i.e. the dE/dx signal will be twice as large in each straw.

As detecting elements, we plan to use straws made from 30 μm thick Mylar or Kapton foil, with a diameter of 4 mm, and a 50 μm diameter anode wire. We have evaluated suitable gas mixtures [21] and propose to use Xe (approx. 50%) + CO_2 (50%), resulting in a maximum drift time of less than 40 ns.

We are driven to using the layouts shown in Figs. 3 and 4 by the need

i) to achieve an azimuthally uniform detector with NO cracks (5% inactive area of the detector would represent a 20% loss in detector efficiency for Higgs $\rightarrow$ 4 electrons);

ii) to reduce material that provokes conversions, which are the bane of TRDs. The proposed construction has very little accessory material interspersed in the detector. In particular, the electronics is located solely on the outer surface. The thickness of the TRD-tracker is thus a few per cent of a radiation length.

The construction for the 'halo' layout (Fig. 3), may use techniques that have been developed and repeatedly utilized for large drift-chamber detectors for storage rings. The figure shows a central TRD-tracker, which could cover $|\eta|$ smaller than or equal to 2.5, as a cylinder with inner radius r_i = 70 cm and outer radius r_0 = 120 cm and a total length of l = 8 m. The full length of the detector would be assembled from several interlocked modules, each one covering the full azimuth.

The mechanical construction for the alternative solution, the 'pinwheel' geometry (Fig. 4), is done in a modular way, each module being an independent, self-supporting unit. The dectector shown here is 70 cm thick, which is necessary for operation at high luminosity. All results shown from here on, where not specified otherwise, refers to this thickness.

As an indication of the tracking capability, we show in Fig. 5 the occupancy of charged particles inside and outside 500 GeV jets, which is almost independent of η in the acceptance of this detector. The occupancy for TR-X rays is of course much lower, approximately only 7% of the charged-particle occupancy.

In addition to the tracking capability provided by the TRD-tracker, a precision measurement of the r-ϕ position of tracks appears to be necessary. One possibility is the use of interpolating-readout 'pad' gas chambers [22]. Resistive interpolation between amplifier taps spaced along an azimuthal cathode strip will give an r-ϕ resolution of 150 μm. A single layer of chambers at a radius of 67 cm for the central region and with pad sizes of ($\Delta\phi \approx 2.8^{o}$) $\times$ ($\Delta\eta \approx 0.015$), will provide better than 1 mm precision for the track position extrapolated to the calorimeter. Several layers of pads might be desirable in order to assist pattern recognition. The total thickness of the pad chamber is ~ 0.01 radiation lengths. There are ~ 70,000 pad channels per layer. Occupancy per channel (including multiple events and track obliquity) would be at the few per cent level. Simulation of such chambers will be included in the MC simulations of system performance, but the development of these chambers is not a part of the current proposal. Our collaboration includes groups at BNL and at CERN who are working to make large low-mass chambers of this type.

4. RESULTS FROM INITIAL TEST OF THE TRD DETECTOR ELEMENTS

In the initial test measurements we concentrated on the evaluation of the different TRD components, i.e. the straws and the foam. In addition, several radiator/straw combinations were studied in a test beam and their e/π discrimination measured.

4.1 Measurements on the straw tubes

As previously mentioned, we intend to use straw chambers as the detector elements for the transition radiation. At this moment, studies are being carried out both on tubes made from Mylar [23] (by a group at Boston University) and on tubes made from Kapton (at the Moscow Physical Engineering Institute). Kapton has the following interesting properties: its rigidity and mechanical strength are equivalent to or exceed that of Mylar; it has exceptional radiation resistance [24]; it has been measured to be ~ 15% more transparent to transition radiation compared with Mylar. With these foils, straws of ~ 4 mm diameter and a wall thickness of 30-35 μm can be fabricated. The diameter of the anode wire is typically 50 to 70 μm.

First, we present test results on the proportional operation of the individual straw tubes. In Fig. 6, we give measurements of the pulse-height resolution and linearity as a function of the gas gain; up to a gain of ~ 10^4 we find the linearity to be good and we observe stable operation. For gas gain exceeding 10^4, the space-charge effects become sizeable and lead to a non-linear response. In Fig. 7 we present results on the variation of

gas gain as a function of the eccentricity of the anode wire inside the straw. The deviations from the ideal coaxial position can be tolerated up to a value of 200 μm, resulting in a change of gas gain of only 2%. We also evaluated the straw-to-straw uniformity of gas gain for a batch of more than 200 straws. The results (Fig. 8) indicate an excellent uniformity with an r.m.s. deviation of the gain of $\sigma \approx 1\%$.

4.2 Evaluation of gas mixtures

We have investigated a number of gas mixtures and evaluated their suitability for TRD operation [21]. For our application, we find that a gas mixture of xenon (50%) + CO_2 (50%) gives an optimum performance. It provides efficient X-ray detection, whilst the total drift time in the straws is less than 40 ns (Fig. 9). This gas mixture was therefore used for the measurements presented in Figs. 6, 7, and 8. This drift time will result in event pile-up from typically two bunch crossings at the 15 ns bunch crossing frequency.

4.3 Ageing tests

Measurements on the radiation tolerance of the straws have been carried out. Preliminary results obtained with the Xe+CO_2 mixture are shown in Fig. 10 [25]. The gas flow through the chamber was limited to a rate of 0.05 cm^3/min; an X-ray generator was used as the radiation source. The monitoring of the ageing was made by comparing the signal from a ^{55}Fe source, using a section of the anode which was irradiated by the X-ray tube with a non-irradiated section. We have observed no evidence of ageing up to a dose of 1 C/cm, which corresponds to ~ 2 years of LHC operation at a luminosity of 2×10^{34} cm^{-2} s^{-1}. Further radiation tests are in progress.

4.4 Transition radiator studies

The Moscow groups have been investigating several foam radiators for their suitability as TR radiators, e.g. polyethylene, polyurethane, polystyrene and carbon foams. As an example we show a microphotograph of a polyethylene foam sample (Fig. 11). The pore diameters and the thickness of the walls of the pores are remarkably uniform. For the purpose of comparison we also measured a regular foil radiator, which was optimized for the test beam energy (20 μm polypropylene foils separated by ~ 280 μm). The radiators were exposed to a 3 GeV beam at Serpukhov, using a test set-up as shown in Fig. 12. Representative results of these tests are shown in Fig. 13. We found that the polyethylene foam gave the best performance, providing a high yield of transition radiation combined with a rather low density. This foam was found to give a TR photon yield that was 15-

20% lower than the one measured with the regular foil radiator. Based on these test results, we estimate that the detector structure proposed here will yield 0.25 detected ionization clusters per centimetre of electron track, to be compared with the still best result of 0.20 obtained by the HELIOS Collaboration [15].

5. FIRST RESULTS FROM THE 180-STRAW PROTOTYPE TEST

In July 1990, a prototype, which was equipped with 180 straws (Fig. 14), was tested by us in the X5 beam of the CERN SPS. The beam provided electrons, pions and muons in the 10 to 100 GeV momentum range. The purity of the beam (hadron contamination of the electron beam and vice versa) was at the 10^{-4} level.

The straws had a diameter of 4 mm and were arranged in 60 rows, separated by 8 mm. The position of three straw-sets in each row was displaced randomly with respect to the preceding one in order to achieve uniform sensitivity of the detector, independently of the impact point of the beam. The straws were operated with a gas mixture of Xe (50%) + CO_2 (50%).

5.1 Pion and electron detection

The tracking capability of the prototype is indicated in Fig. 15, showing the accuracy of track reconstruction for isolated pions and electrons. The particles traversed 30 straws on the average. We measure an angular resolution of σ_θ = 1.5 mrad and a position resolution of σ_x = 0.4 mm. In Fig. 16, we show the energy spectrum recorded in a straw, resulting from the traversal of one electron, one pion, and two simultaneous pions (10 GeV particle momentum). The contribution to the energy deposition from TR photons is clearly seen in the high-energy tail of the spectrum. Particle identification, recognition of conversions and overlapping tracks are based on the information contained in the energy spectra.

Three different thresholds are used for measuring the ionization clusters in each straw. The first threshold level (TH_1 at 0.2 keV) gives about 90% efficiency for relativistic particles and would be used for tracking. The second threshold level (TH_2 at 1.5 keV) is located between one- and two-particle dE/dx distributions; it has ~ 50% efficiency for minimum-ionizing particles and ~ 80% efficiency for conversions. The third threshold level (TH_3 at ~ 4.5 keV) corresponds to ~ 90% efficiency for TR X-rays.

The contribution of TR photons, with an average energy of 7 keV, is measured by the frequency of energy deposits exceeding the highest discriminator threshold. As an example (Fig. 17), electrons of 10 GeV produce, on the average, 9.5 energy deposits above tTH_3 for 40 straws crossed, whereas pions at the same energy exceed this threshold only in 2 straws.

5.2 The $\gamma = E/mc^2$ dependence of the TR yield

We have measured the TR yield in the γ–interval $\gamma_{min} = 70$ to $\gamma_{max} = 6 \times 10^4$, using the following beams:

- pions at 10, 20, 50, and 75 GeV,
- muons at 110 GeV,
- electrons at 10, 30 GeV.

The results are presented in Fig. 18 and indicate both the contribution of the relativistic rise in the energy loss dE/dx ($E_\pi < 50$ GeV, $\gamma < 350$), and TR photons ($\gamma \geq 350$).

5.3 TRD identification of isolated particles

In Fig. 19 we exhibit, the capability for electron/pion discrimination. We show several two–dimensional scatter plots of the frequency of high–energy deposits ('clusters') ($E > TH_3$) against 'single particle hits' ($TH_1 < E < TH_2$). The various scatter plots correspond to the actual situations encountered in an experiment, such as electrons, single or multiple pions, and conversion pairs. Quantitatively, the measured rejection power is given in Fig. 20 for pions in the range 10 to 140 GeV. Also shown are the MC predictions for pions in the range 1 to 140 GeV, which are in good agreement with the test beam data. Rejection factors of better than 100 are obtained for $\varepsilon_e = 90\%$ over the full pseudorapidity range and for $E_\pi = 25$ GeV.

6. MONTE CARLO STUDIES OF SYSTEM PERFORMANCE

6.1 Tracking performance

We have conducted Monte Carlo studies of the basic conceptual design, using the ISAJET generator [19]. In particular, we studied the electron identification potential of our proposed TRD in the presence of a very high charged-particle multiplicity environment. High-p_T (p_T > 100 GeV) two-jet events were generated, to which were superimposed a 25 GeV electron and a background of 40 minimum-bias events. Such an event, as recorded in a TRD section, is shown in Fig. 21a (all hits with energy above TH_1 = 0.2 keV shown) and Fig. 21b (hits exceeding TH_3 = 5 keV). The cleaner view (Fig. 21c) is obtained after the application of a track-finding algorithm.

The identification of photon conversions in the TRD is also in progress. This background is recognized in the following way:

- Before the conversion point, straws along the trajectory will show the random occupancy level.
- Straws after the conversion point will show a energy spectra that is characteristic of two-charged particles.

In addition to the three-level energy deposition criterion, our tracking algorithm imposes the additional constraint of consistency of energy deposits (i.e. thresholds exceeded) along the track, with a specific particle hypothesis. This 'extended' three threshold algorithm was used in the definition of electron track candidates (Fig. 21c).

6.2 Rapidity dependence of the performance of the TRD-tracker

In Fig. 22 we show the scatter plot for the N_{12} versus N_3 populations, similar to the distributions shown in Fig. 19 for isolated particles. These distributions show, in more detail, the TRD rejection power under conditions of very high luminosity ($\sim 2 \times 10^{34}$ cm^2 s^{-1}). The same information is represented in one-dimensional form in Fig. 23, showing the TRD rejection as a function of the pseudorapidity η for various luminosities.

6.3 Accuracy of vertex reconstruction

Owing to the orientation of the straws in the plane perpendicular to the direction of the colliding beams, a relatively good localization of the interaction vertex and of the impact

point on the calorimeter face is possible (see Fig. 15). We have simulated the electron track reconstruction for $L = 2 \times 10^{34}$ cm^{-2} s^{-1}. The electron track was defined by at least six straws with an energy deposit $E > 5$ keV. The corresponding resolution in the z-direction is shown in Figs. 24a and 24b for vertex and calorimeter surface respectively.

6.4 Electron identification inside jets

One of the objectives of the TRD is to have the possibility to identify electrons close to the axis of high-p_T jets. A preliminary evaluation was carried out, simulating two-jet events ($E_T^{jet} > 100$ GeV) at a luminosity of $L = 2 \times 10^{34}$ cm^{-2} s^{-1}. Results are shown in Fig. 25 for four intervals of pseudorapidity.

6.5 Tagging of particles with large Lorentz factors

With the aid of the TRD it is possible to identify not only electrons but also other charged particles with $\gamma > 10^3$. Of particular interest is muon tagging by the TRD, to link up to tracks from the muon spectrometer. The achievable hadron rejection factor, for 90% muon efficiency, is shown in Fig. 26 as a function of the muon energy for two values of the polar angle.

These Monte Carlo results, while not exhaustive, indicate the power and the flexibility of the integrated TRD-tracker approach to identifying electrons and in rejecting a variety of potentially troublesome backgrounds.

7. THE TRD AS A TRIGGERING DEVICE

We conclude that the proposed TRD will be built having an active triggering function at a second level in mind. As an integral part of the straw electronics, active ('intelligent') elements will string together digitizings into track candidates. Based on statistical properties of pulse heights, they will thus be able to determine an *electron likelihood* for every track found.

The trigger is called 'second level' because it relies on a preceding fast 'first-level' trigger, based on calorimetric information alone. (If the detector is suitably built and if the TRD has the required performance, then a muon trigger function could operate in an analogous fashion, but we will ignore this possibility in the following.) The required frequency of executing this second-level algorithm is, of course, strongly dependent on the rate of first-level triggers. Based on the expected rates of physics discussed above, we assume that the first-level trigger operates on the calorimeter towers at beam-crossing

frequency, and that it presents electron candidates every 10 μs on the average. The tentative data-flow design discussed below is therefore constrained for second-level decisions based on TRD information found at a 100 kHz frequency, confirming (or not) the tentative first-level electron decision. This rate is relevant, and must be attained for a dead-time free operation of the trigger, but it is not identical to the decision-taking time: if all relevant data are kept in suitable buffers, then a longer time span is available for the final trigger-choice of each electron candidate (the *latency* of the system). We assume that a latency of several hundred microseconds can be tolerated.

Note that, in the discussion below, we consider the *trigger* aspect of the TRD as a pure *Slave* function, invoked only by the first-level tagging of electron candidates, and operating only in regions indicated by the first-level device. Beside this trigger function, the system will have to possess a complete passive readout, which makes it a general tracking device at a higher level or off-line.

In order to minimize the number of special developments, our intention is to embed, as an intelligent device, an architecture that is fully or partly available from industry [26]. Our most promising choice at this early stage of discussion appears to be a massively parallel system marketed by Aspex. Its product, called ASP (for Associative String Processor), is one of the many emerging solutions for massively parallel processing. It combines concepts which have been well known for a long time, but which have not been brought together into a commercially available system. The processors are called 'associative' because they have a fast (one-dimensional) connection line and pattern-matching instructions, allowing a fast addressing mode by register content.

The basic chip of current ASPs carries 64 processing elements (APEs), whose internal design can, within limits, be adapted to the application (e.g. the depth of data memory, or the number of activity bits). Chips are at present grouped into hybrids of 16 chips, or 1024 processors. Multiple hybrids are connected into strings. The higher-level controller, which issues the commands to APEs (every string of processors works in lockstep), is off-hybrid and can be custom-designed. The string length and the implementation of multistring systems are other free design parameters, to be adapted to the TRD. At present, Aspex is engaged in a formal collaboration with CERN, Saclay, and IN_2P_3, to produce several application-oriented boards with multiple strings of processors. The 1991 goal of this collaboration is a total of 65,000 processors; for the purposes of a TRD trigger system, a total number of processors much higher than this goal has to be envisaged.

In the following, we will concentrate our discussion on one specific technology, the ASP solution, although its feasibility has yet to be demonstrated, and other image-

processing devices may eventually emerge as serious competitors. From our past collaboration with Aspex, it is our belief that enough experience exists to implement an ASP solution. Our discussion below, however, is kept at a functional level as much as possible. We consider only the 'halo design', which is the more complicated one.

7.1 Overall architecture

For all possible solutions, our goal has to be a second-level trigger architecture which is scalable (can follow later expansions of the detector or adapt to more complex trigger algorithms); provides software parametrization of trigger parameters (can follow changing beam and physics environments); maintains flexibility (i.e. can follow the evolution of understanding of the detector's possibilities); is maintainable (i.e. can be serviced and provides sufficient information for monitoring and permanent control); and is itself fault-tolerant (i.e. malfunction degrades the system performance, but does not cripple it). Last but not least, economies of costs, power, and space will have to be considered.

Massive parallelism, as advertised by its proponents, can provide the equivalent of extraordinary computing power. However, to which problem-classes parallelism is restricted, is a lesson yet to be learnt. It is generally accepted that many problems get entangled in the difficulty of organizing the data flow efficiently. This is particularly true of SIMD architectures (for Single Instruction Multiple Data), of which the ASP is a representative. To supply data to a very large number of processors, which subsequently use them in lockstep for a comparatively simple computation, is a far from trivial problem, and one that is impossible to solve in general. SIMD machines that are marketed as complete systems will consequently tend to ignore the issue, thus restricting their use to compute-intensiveapplications.

The TRD does not possess a natural geometrical subdivision that would provide a natural parallelism for finding tracks. The very choice of straws with one-sided readout, and the desire to maintain a general tracking capability (by stereo views), are acting against trivial parallelism. Knowing the spatial region of an electron candidate seen in a calorimeter tower identifies a group of straws, but every straw potentially contributes also to other spatial regions. *Spatial* parallelism, therefore, is at best a partial one, and a function of data grouping must be embedded in the necessary transmission and collection hardware.

We assume that, for reasons of performance limits, *temporal* parallelism will have to be a necessary complement; parallelism in time results in simultaneous treatment of different events. We may further want to exploit parallelisms inherent to the chosen algorithm: if the histogramming of hits with different cuts of pulse height is necessary, then

the accumulation may take advantage of parallelism by obtaining different bins and/or different cuts simultaneously.

The algorithms in a string of ASPs can be assumed to be data-independent, in the sense that the execution time is a constant (SIMD systems, unlike classical von Neumann machines, do not find branch instructions or variable-dependent loops natural). Data transmission also is considerably simplified if it is assumed to be fully synchronous, as the need for scheduling and arbitration units disappears. We therefore assume that data transmission starts, immediately after the first-level trigger gate, with a derandomizing buffer, and the synchronous operation is maintained until completion of the second-level trigger.

The following discussion refers mostly to the data flow through the second-level trigger, which is a simple Slave device serving only the first-level trigger candidates. The data flow, does of course contain a parallel full data path for TRD raw data, potentially used in general tracking. Note that such full data, even if not needed for any other purpose, would be mandatory for recording samples of events, which are needed in order to maintain full control of the triggering performance. The transmission rate of full data, however, can be assumed to be lower than the 100 kHz after first level, by a factor given by the combined effect of all second-level triggers.

In coding the algorithm, some architectural details of ASP strings are likely to be used: the fact that along any given track the maximum number of hits remains within narrow limits (~ 30) could be used to advantage by storing all potential hits into ASP data words (currently 64 bits available). Likewise, it is conceivable that the ASP string length is eventually optimized according to the specific data structures at the TRD. Note that we have started modelling (simulating) the data flow and the ASP at a functional level, and that this modelling is an important part of the design cycle (at present we use the commercial package Verilog, complemented by an Aspex-proprietary ASP simulator).

7.2 Front-end embedding

It is premature to make precise assumptions concerning the passage of information from the drift wires to a second-level triggering and storage device. A wide variety of different solutions are being researched in the context of LHC, and they may be as different as digitizing (with few-bit precision) at bunch-crossing rate, with subsequent transmission via high-rate (multiplexed) fibres, or storing the analog information locally in switched capacitors, and transmitting with zero suppression, once a first-level trigger has been obtained and broadcasted.

For the trigger concept of this Proposal, it is sufficient to assume that TRD straw data are stored, grouped by criteria dictated by geometry, in a suitable number of digital data buffers (e.g. 1024), at a defined time span after the relevant bunch crossing. These buffers need to be deep enough to allow them to act as the data synchronizing unit discussed above.

7.3 Data collection, transmission, and regrouping

From a data grouping dictated by cable/fibre and geometrical considerations alone, data now have to be transmitted to larger buffers, eventually allowing the access to all straws participating potentially in second-level trigger algorithms. The basic consideration here is that commercial transmission lines should be used; overall data rates dictate the use of standard fibres and multiplexing, and of commercial protocols. This makes it convenient to imagine the TRD storage and triggering electronics as being located at a distance from the detector. A logical subdivision of the straw volumes into azimuthal sectors and rapidity blocks is introduced at this stage. However, as such a division can not be made without overlap due to detector construction, it does not need to match the pattern of calorimeter (trigger) towers more than crudely. Our present model is shown in Fig. 27.

Conceptual units called *Blocks*, will combine the data from a fixed number of de-randomizing units *(Sectors)*, grouping data in a rudimentary geometric way. A subsequent fast (by look-up techniques) *spatial* rearrangement constructs up to a maximum number of *windows* for each event defined by the maximum number of first-level triggers. In a subsequent *temporal* rearrangement, a *router* serves data to a number of *processor banks* in turn. This allows the data flux to be sufficiently reduced for narrower *roads* to be selected, and provides the desired scalability related to the processor performance.

7.4 Decision algorithm

The I/O into the data registers of APEs can be achieved with a large degree of parallelism, but it cannot overlap with computation, and takes up a sizeable fraction of the 100 μs which is our present goal for the execution of the triggering algorithm in a string of APEs. We therefore envisage to have strings that alternate between a *'reading and reshuffling'* mode and a *'histogramming'* mode that corresponds to the track-finder proper (we assume that the track-finding core is a histogramming algorithm). Details of both the data input and the algorithm execution will have to await for a more advanced modelling. The track-finding itself is based on encoding (mostly in transmission tables) the spatial

path of tracks in three dimensions, in terms of straw/plane numbers, thus defining 3D 'roads' in which the actual hits are histogrammed. Restricting these roads to the limited number of first-level candidates allows a solution that is within the constraints of economy.

8. PRINCIPAL DEVELOPMENT EFFORTS

We describe below the principal areas on which we wish to focus our R&D effort.

8.1 Mechanical developments

Several areas require attention for the construction of the TRD-tracker.

As mentioned in Section 3, two possible geometric arrangements are envisaged: the 'pinwheel' and 'halo' geometries. The mechanical construction for the pinwheel geometry is done in a modular fashion, with each module being independent and self-supporting.

Two possible schemes are under consideration for the construction of the halo detector (Fig. 28). In the first one, the detector would be assembled from several interlocking modules, each one covering the full azimuth. We prefer to tension the individual tubes slightly (approximately 100 g per tube) in order to straighten them and to define in this way the geometrical location of the detecting elements. The direction of the straws in alternate layers will be mirror-inverted, ensuring overall mechanical stability of the barrel and the possibility for second coordinate determination by large-angle stereo. The 'outer' straws, which terminate at the intermediate radius are mechanically prolonged with thin carbon fibres reaching to the inner radius, so that all straws are mechanically identical. In the second construction method, half-straws are formed from very thin aluminium-covered Mylar foil (~ 6 μm of aluminium) on a backing of foam material. Two half-modules are assembled as shown in Fig. 29, with a thin Kapton foil between them. This foil has long slots cut into it, corresponding to the active region of the finished straws. The wires are fixed relative to the foils by means of the small bridges between the slots. In this way the wire can be soldered to the Kapton foil support in a conventional manner. In addition, the gas inlets and outlets are easily connected to gas manifolds.

Studies of the properties of the multi-straws must be pursued. Extensive tests of pulse shapes, drift times, irradiation tolerance, and other properties will be required for the various options in straws and gases. This work will be pursued at Moscow and CERN,

drawing upon broad experience in building and operating proportional-straw tracking devices [23,25].

Continuing study of foams for the radiator material is required. Foams have already been used in some experiments [27]. Foam is very appealing for the simplicity of the radiator structure, for the mechanical support and rigidity it can lend to the straw assembly, and because its TR response is independent of the direction of the incident particle. Foams are available with a wide variety of physical characteristics [28]; we are continuing our search to find a material with sufficiently regular cell size and wall thickness appropriate for the LHC regime. The Moscow groups will continue their work in this area. Open-cell foams for the radiators could be interesting as a way to address cooling problems.

8.2 Electronics developments

The signal processing and the interface to the trigger processors represent, in our view, the most critical element of our proposed detector system. Areas of particular concern to us are

- the concepts of signal processing that are consistent with the performance goals of the detectors: sensitivity, noise, speed, reliability, and power dissipation of the front-end;
- the readout architecture, allowing high-speed communication with the trigger processors (to tag electron candidates and very high-p_T particles, and to reject background of 'false' electrons).

Whilst all of the above criteria will have to be successfully incorporated, we feel that overriding priority has to be given to reliability. In our view, the highest obtainable reliability implies a minimum of readout functionality on the detector — in marked contrast to concepts normally expressed in 'workshops'. The only signal-processing elements we are prepared to tolerate are transmission elements (e.g. preamplifiers) for channelling the straw-tube avalanche signal to off-detector receivers for further processing. All other signal processing functions, such as multiplexing, signal storage, etc., should be located away from the detector.

In addition to utmost simplicity —synonymous with utmost reliability— our readout must also satisfy a second crucial requirement, namely that of very low mass (a maximum of only a few percent of a radiation length can be tolerated). This transparency to electrons and photons is necessary, as we conceive our TRD-tracker to be compatible with an outer high-resolution pixel detector of the pad-chamber type.

8.2.1 Front-end signal processing

Reliability in signal processing, simplicity in functionality, and transparency to photons then determine our overall readout strategies. In the following, we describe two independent concepts, which we propose to study and develop.

The first approach uses a novel concept of optical-fibre readout. We plan to investigate the transfer of signals into an optical fibre by means of an electro-optical modulator (Fig. 30). An optical signal is brought to the detector from an external light-source and is used to power 16 to 32 modulators on a single substrate. Each modulator is excited by the electrical signal from the straw tube, with the corresponding modulated optical signal exiting on an optical fibre. We are at present evaluating the noise level in such modulators to see whether a preamplifier is required or whether the anode of the straws could be connected directly to the modulator. The former is still very advantageous, since the modulator is a very high impedance load, needing a little power to drive it, while preserving the rise-time of the output signal over as long a fibre as may be necessary for generating the required delay for the first-level trigger. Even with one fibre per channel, the mass of the complete fibre readout is quite acceptable. If no preamplifier is needed, it would present the added advantage of eliminating transistors entirely from the front-end of the TRD-tracker.

The radiation resistance of the optical modulators themselves needs further studies, although it is expected to be good. The $LiNbO_3$ substrate, the Ti-diffused waveguides, and the Au-deposited electrodes all seem to be intrinsically radiation-hard materials. The infrared wavelengths used, probably ~ 1.3 μm, are those for which absorption induced by the radiation is low compared with the ~ 40 mm scale of the waveguide length in the modulator. The quartz fibres used for the light transmission have been thoroughly studied by a number of groups. We know that these fibres are tolerant to a dose of at least 10^7 Gy, and we do not expect radiation problems.

The second concept that we wish to develop further is 'classic' and conservative. Only preamplifiers are mounted directly at the end of the straws on the outer cylinder at the radius of $r = 120$ cm. Each preamplifier has to be connected with cables to off-detector circuits (shapers, storage elements, etc.) for further signal processing and triggering. This concept poses the challenges of developing low-power fast preamplifiers and adequately low-mass cables. In the following we describe a solution that can be implemented with present technology and could be tested approximately one year after the approval of the Proposal.

Several ASICs (application-specific integrated circuits) with performance specifications approaching our needs are already available or are in an advanced production phase, as summarized in Table 1. Given the considerable activity in this field, we consider it unnecessary to start a further independent development at this moment. In our opinion it will be more effective to carry out an engineering analysis of our specific application, and to evaluate which ASIC, among the several contenders, would most closely approach our needs and could be adapted to our application. Engineering help for this evaluation as well as possible modification and the necessary liaison with the group who would carry out the ASIC adaptation, is one of our requests to CERN.

Having established -in our view- a credible approach to the front-end signal processing, we must ask whether it is possible to connect these preamplifiers through adequately low-mass cables, to the off-detector signal processing. In the following, we discuss a scheme -again using today's technology- that indicates that indeed it should be feasible.

The technique we propose to use is based on microstrip transmission lines, fabricated with printed-circuit manufacturing methods. Such methods have already been used repeatedly, most recently, for example in the DELPHI VSAT, the Jet-Set Fast RICH, the UA2 Si-pad readout, and the ZEUS Si-readout. For discussion purposes, we consider signal transmission lines having the following characteristics:

Type of transmission line:	central conductor between two parallel ground planes
Characteristic impedance:	$Z \approx 50\ \Omega$
Substrate material:	Kevlar, 50 μm thick
Dielectric:	PE-foam, $\varepsilon \sim 2$ (?), thickness 2×250 μm
Electrodes:	Cu; ground electrode 30 μm
	central conductor 60 μm
Width of electrodes	ground electrode 1500 μm, central conductor 300 μm
Attenuation (at 50 MHz)/m	1.2 dB (estimate)

The dimensions of the transmission line are determined by the value for the attenuation, deemed acceptable. Using a transmission of the above characteristics, we imagine NOT linking the readout cables directly to the detectors' ends, which would imply a maximum length of ~ 4m. We prefer to consider two small annular slots surrounding the TRD-tracker at a distance of ± 130 cm and ± 260 cm. In this way the cables would be directed in a sheet around the circumference of the TRD-tracker, up to the slot in the pad detector, then slotted through the pad detector and prolonged into the 'end-plates' with a somewhat thicker and less lossy cable. Arranged in this way, the cable sheet would represent, on the average the equivalent of 0.6 mm Cu or ~ 3% of a radiation length.

We stress that this scheme should only be considered as an indication that the low-mass connection is a manageable problem. No optimization's of dimensions versus loss has yet been made. On the time scale for the LHC, more ambitious approaches should also be followed up, e.g. the use of aluminium in lieu of copper in order to reduce the amount of material further.

In summary, we propose to pursue two technically very different strategies: the optical modulator solution is characterized by its conceptual simplicity, but requires substantial R&D efforts; the electronics preamplifier solution can be expected to perform in the LHC league and can be realized quickly for advanced prototype testing. Both solutions have the virtue of removing the post-processing electronics and triggering from the detector, and can be analyzed and developed without interference with the detector and front-end electronics.

8.2.2 Off-detector electronics

The two transmission options discussed above provide us, off-detector, with a continuous flow of data in analog form. For the purposes of further processing, this data has to be:

- buffered until a first-level trigger decision has been reached and broadcast;
- integrated over the necessary time so as to provide a best estimate of the signal for each wire in every bunch crossing;
- digitized in a crude way (three thresholds);
- buffered to obtain the derandomizing effect;
- channelled through a variety of transmission/switching/collection components according to Fig. 27, until a second-level decision has been reached and data are either overwritten or passed on to an event-building unit.

These functions will most likely lead us to consider VLSI solutions, at least for the components that are logically closest to the detector. The ASICs will be the only economically viable and reliable solutions for several hundreds of thousands of individual channels. We can assume that among the various projects now under way in the context of the LHC (and SSC) microelectronics developments, at least up to and including the digitizing function, HEP-based components and associated expertise can be found, albeit with some adaptation for the specific task of the TRD (e.g. few-bit FADCs). For the digital transmission, buffering, and switching components -as for the processing units executing the trigger algorithm proper- we will attempt to rely, as much as possible, on solutions coming from industry: telecommunications, main-frame computer networking, and HDTV (high-definition television) are areas in which components for our task can be found.

High-bandwidth point-to-point connections with minimal protocol can be provided by industrial hardware such as that used in FDDI or HPPI, or even by future transputer links. Fast switching components are available from some computer manufacturers; some of them are already being explored by Fermilab staff in the context of generic studies for the SSC. Buffering components are part of many modern video-oriented developments. As for processing units, we consider various image-processing devices and SIMD arrays as serious candidates, but do not exclude that standard microprocessors of the future could also be appropriate.

During the first year of the project, we plan to concentrate on the evaluation and simulation of possible concepts. Our TRD project would provide one of the first applications for new 'LHC'-style processing. Although our application is detector-specific, the experience obtained should be valuable for data processing for several different detector components.

As one example of our working mode, we mention that we are at present carefully evaluating the ASP machine as one possible processor technology. This technology is currently supported, in a detector-independent collaboration (MPPC: Massively Parallel Processing Collaboration), by Saclay, IN_2P_3, CERN, and the producing company Aspex, together with several application-oriented institutes. We would be prepared to participate actively in further similar technical collaborations, e.g. exploring fast industry-supplied links or switching components. As in the case of the MPPC, such collaborations are likely to produce feedback for industrial products of the future, and would allow the necessary build-up of know-how inside our high-energy physics institutes.

At the present stage we can make the reliable evaluation of the needed resources (personnel and finances) for only the first year of this project (see Section 9). Before the end of the first project year, we will submit a status report and an updated request for personnel and budget.

8.3 Simulation of detector systems

Complete simulations of the various options for the detector configuration will be necessary in order to evaluate the advantages and disadvantages of each feature and to assess the system performance in the LHC environment. Some Monte Carlo programs for simulating the TRD-tracker have already been developed in Moscow. Over the past years, this simulation tool has been honed to the point of providing accurate performance evaluation and optimization of one system design. Simulation at the signal level has

already been implemented for the development of the electronics and triggering components.

9. MILESTONES

In this section we present the milestones of this development project. For 1990 we have indicated, in some detail, the specific work in progress and the institutes that are principally involved in each task. The programme for the subsequent years is presented in somewhat less detail.

By early 1991 we anticipate having a test detector with approximately 1200 straws and discrete electronics ready for beam tests in a 450 GeV beam at CERN. In addition, we plan to equip a few hundred channels with new electronics (optical modulators and fast-shaped electronics). The purpose here will be to verify the TRD and the tracking performance in a simulated high-luminosity environment, and to test the engineering concepts for manifolding and support. By mid-1993 we plan to have a full-scale prototype of a TRD-tracker half-sector, with readout and associated trigger processors. This will be installed in the test area together with a pad chamber and the BNL/CERN liquid-argon calorimeter, and will be subjected to full system performance tests.

This programme is carried out in collaboration with a group from Boston University (J. Beatty, E. Booth, J. Shank, J.S. Whitaker and R. Wilson). In particular, the 1990 test of the 180-straw prototype was carried out together with this group. We will continue to co-operate closely, and to emphasize complementary studies, and we plan to collaborate on the 1991 test. For this reason we have listed Boston University as a contributor for 1990.

Activities in progress during 1990

- Assessment of mechanical engineering issues: structural support of the modules, gas manifolding, heat flow (Moscow).
- Monte Carlo study of the performance of the system, and refinement of the conceptual design (BU, Moscow, Dubna).
- Laboratory tests of straw performance, including drift times, and signal shape, using different xenon mixtures (BNL, BU, Moscow).
- Design and tests of different radiators (Moscow).
- Radiation damage studies of straw/radiator assemblies (BU, Moscow).
- Study of readout architecture and triggering requirements, in conjunction with the LHC calorimeter R&D and LHC trigger groups (BNL, CERN, Dubna).
- Beam tests of the 180-straw prototype (BNL, BU, CERN, Lund, Moscow)

- Preparation of a 1200-straw test module:
  - mechanics (Moscow, Dubna),
  - electronics (BNL, CERN, Lund, Dubna),
  - test facilities (CERN).
- Evaluation of readout options (BNL, CERN, Lund).
- Set up a test station for trigger development tests (CERN).

Goals for 1991

- Finish construction, set up, run, and analyse a 1200-straw test system.
- Run the 1200-straw test with a pad-chamber and calorimeter.
- Demonstrate the elements of the trigger architecture.

Goals for 1992

- Design and start construction of a 15,000-straw prototype detector.
- Engineer trigger processor for a 15,000-straw system.

Goals for 1993

- Complete the trigger processor for a 15,000-straw system.
- Test the 15,000-straw prototype detector system, with pad-chamber and calorimeter.
- Analyse the 15,000-straw test results and compare them with simulations.
- Iterate the design for the final detector.

Sharing of responsibilities and requests

We ask to keep the NA34 liquid-argon calorimeter with the cryogenic system, the control room, the muon magnet with cryogenic system, the readout electronics, and the on-line system, for the duration of the programme in order to permit the system tests described in this proposal.

Requests for 1990:	kSF
– Installation costs, operation of the 180-straw test (CERN):	15
Digital oscilloscope (will be shared with other groups in ECP-Division) (CERN):	40

Responsibilities and requests for 1991:

– 1000 fast preamplifiers and shaping amplifiers: Estimated costs expected to be contributed by BNL and Lund.	[110]
– 1000 peak-sensitive ADCs; available from NA34.	
– 100 channels with optical modulator readout; expected to be provided by the US-collaborators:	[355]
– 100 channels with very fast, multiple-threshold cluster counting (CERN):	50
– Construction of the 1200-straw prototypes; joint responsibility of Dubna and Moscow Institutes; estimated cost if development and construction were carried out at CERN:	[300]
– Low-dispersion cables, connectors for 1200 channels (CERN):	90
Interfacing of readout to trigger electronics (CERN):	50
Mechanical studies in preparation for the 15,000-straw detector (CERN):	50
– Installation, operation of the 1200-straw detector (CERN)	40
Xe-gas for the operation of the 1200-straw detector (2000 l) (Moscow)	[20]
– Financial support for three Soviet physicists (two man-years) (CERN)	100

Request to CERN for the first two years:	435 kSF
Contribution of non-CERN collaborators:	580 kSF
Computer time at CERN (40% of total time needed):	1000 hours
Test beam requirement in 1991	6 weeks

(A beam of identified pions and electrons in the momentum range 5 GeV to 150 GeV is needed with an intensity of ~ 10^5 particles per burst and square centimetre.)

Requests for 1992

We consider it premature to present itemized requests for 1992 at this moment. The activities during the coming 10 months will result in a clarification of the mechanical, electronics, and trigger specifications. Therefore, we propose to submit a Status Report and a documented request for 1992, to this Committee, by the middle of 1991.

Acknowledgements

We wish to thank M. Botlo, who participated in the studies on the trigger architecture and made important contributions to the 1990 TRD tests. We are grateful to D. Froidevaux for many clarifying discussions on the role of a TRD in an LHC experiment. His careful reading of the manuscript resulted in considerable improvements.

References

[1] See for example: J.H. Mulvey ed., Feasibility of Experiments at High Luminosity at the Large Hadron Collider, (CERN 88-02, Geneva, 1988).

[2] J. Franck and V. Ginzburg, J. Phys. USSR 9 (1945) 353.

[3] See for example: M.L. Cherry et al., Phys. Rev. D10 (1974) 3594;
Artru et al., Phys. Rev. D12 (1975) 1289;
G.M. Garibian et al., Nucl. Instrum. Methods 125 (1975) 133.

[4] T. Ludlam et al., Nucl. Instrum. Methods 180 (1981) 413.

[5] C.W. Fabjan et al., Nucl. Instrum. Methods 185 (1981) 119.

[6] J. F. Detoeuf et al., Nucl. Instrum. Methods 265 (1988) 157.

[7] M. Holder and H. Suhr, Nucl. Instrum. Methods 263 (1988) 319.

[8] R. Ansari et al., Nucl. Instrum. Methods 263 (1988) 51.

[9] Y. Watase et al., Nucl. Instrum. Methods 248 (1986) 379; Transition Radiation Detector for VENUS Experiment at TRISTAN , KEK preprint 87-29 (1987).

[10] H.J. Butt et al., Nucl. Instrum. Methods 252 (1986) 483.

[11] R.D. Apphun et al., Nucl. Instrum. Methods 263 (1988) 309.

[12] A. Vacchi, Nucl. Instrum. Methods A252 (1986) 498.

[13] J. Cobb et al., Nucl. Instrum. Methods 140 (1977) 413.

[14] I.A. Denisov et al., preprint FNAL 84/134-E (1984).

[15] B. Dolgoshein, Nucl. Instrum. Methods 252 (1986) 137.

[16] G.B. Yodh et al., Proc. DPF Summer Study on the Design and Utilization of the SSC, Snowmass, 1984 (Amer. Inst. Phys., New York, 1985), p.523.
G. Brandenburg et al., Proc. DPF Summer Study on the Physics of the SSC, Snowmass, 1986 (Amer. Inst. Phys., New York, 1987), p.420.
T. Akesson et al.,Proc. Workshop on Experiments, Detectors and Experimental Areas for the Supercollider, Berkeley, 1987 (World Scientific, Singapore, 1988), p.472.
T. Akesson et al., *in* The feasability of experiments at high luminosity at the Large Hadron Collider (CERN 88–02, Geneva, 1988), p.31.

[17] H. Grassler et al., Simultaneous Track Reconstruction and Electron Identification in the H1 Radial Drift Chambers; paper presented by J.B. Dainton at the Workshop on $4-\pi$ Tracking Systems for the Superconducting Supercollider, Vancouver, 1989.

[18] J.–P. Repellin, contribution to the ECFA Calorimetry Study Group for Aachen 1990. The number quoted in the text depends on the calorimeter granularity and pile-up effects due to luminosity and signal shaping time.

[19] F.E. Paige and S.D. Protopopescu, Brookhaven report BNL-38034 (1986).

[20] P. Nason, private communication.

[21] J. Fischer et al., Nucl. Instrum. Methods 238 (1985) 249.
B. Dolgoshein et al., Gas Mixtures for Transition Radiation Detectors at High-Luminosity Colliders, preprint CERN-EP/89-161 (1989).

[22] A. Angelis et al., Nucl. Instrum. Methods A283 (1989) 762.

[23] S. Ahlen et al., Phys. Rev. Lett. 61 (1988) 145;
A. Tomasch et al., Nucl. Instrum. Methods A241 (1987)265.

[24] H. Schonbacher in ECFA Study Week on Instrumentation Technology, Barcelona 1989, CERN 89-10, Geneva, 1989, p. 359.

[25] V. Bondarenko et al., Preprint Moscow Phys. Eng. Inst., in preparation (1990).

[26] S. Lone, R. K. Bock, Y. Ermolin, W. Krischer, C. Ljuslin, K. Zografos, Nucl. Instrum. Methods A288 (1990) 507.

[27] See for example, M.L. Cherry, Phys. Rev. D17 (1978) 2245, and references therein.

[28] D.A. Wrobleski et al., Los Alamos National Laboratory report LA-11271-MS, July 1988.

Figure captions

Fig. 1 Cross sections for different processes for real and false electrons as a function of an isolation cut $E(\Delta R) < 10$ GeV, for $p_T^e > 25$ and 50 GeV. False electrons originate from the spatial overlap of γs with hadrons, assuming a spatial accuracy of $\sigma = 5$ mm, and using a 4σ cut (see text for explanations).

Fig. 2 Cross section through a conceptual TRD. The straws are embedded in the radiator material, e.g. polyethylene foam.

Fig. 3 Possible TRD-tracker layout (halo design).
Figure 4a shows the overall dimensions along the beam, with an η coverage of $|\eta| \leq 2.5$; in Figure 4b a cross-section of the halo detector shows the direction of the straws and the arrangement of long and short straws.

Fig. 4 Alternative layout, cross-section, of the TRD-tracker in an experiment (pinwheel design). This layout is a consequence of our belief that the electronics should be located outside the active detector.

Fig. 5 Occupancy of straws by charged particles as a function of the angular separation from the jet axis. The occupancy due to TRD clusters is approximately an order of magnitude less. The additional occupancy from 40 'pile-up' events is also shown.

Fig. 6 The energy resolution (FWHM of pulse-height spectrum of ^{55}Fe) and the ratio of signal amplitudes at 1.7 keV (Xe escape peak) and 5.95 keV versus the gas gain. The results are shown for 20 μm and 50 μm anode wires.

Fig. 7 The dependence of the energy resolution and gas gain for 5.95 keV photons as a function of eccentricity Δx of the anode wire.

Fig. 8 The distribution of the average gas gain for a sample of 240 straws. The r.m.s. width of the distribution is ~ 1%.

Fig. 9 The total drift-time measured in straws as a function of CO_2-concentration and anode wire diameter. The Xe-fraction was kept constant at 0.5 atm.

Fig. 10 The radiation tolerance of the straws is indicated by the change in gas gain as a function of the total accumulated charge on the anode. Shown is the ratio of the signals, induced by an ^{55}Fe source, from an irradiated and a non-irradiated section.

Fig. 11 Microphotograph of the polyethylene foam that was tested at Serpukhov. The cell diameter is (200 ± 70) μm, and the wall thickness is (15 ± 5) μm. The foam density is ~ 67 mg/cm^3.

Fig. 12 Layout of the Serpukhov test for measuring the TR yield from foam and from periodic foil radiators.

Fig. 13 The comparison of several radiators. The abscissa gives the probability for pions to exceed a certain charge−threshold; the ordinate gives the corresponding value for electrons. Results are shown for one radiator/detector layer. The solid curves represent our Monte Carlo calculations and the different points refer to measurements of the following radiators:

▼ − radiator made of regularly stretched polypropylene foils;
△ − polyethylene foam (0.059 g/cm^3)
○ − polystyrene foam (0.110 g/cm^3)
● − carbon foam (0.080 g/cm^3)
× − polystyrene foam (0.040 g/cm^3)
▽ − polyurethane foam (0.055 g/cm^3)

Fig. 14 The geometrical structure of the 180−straw TRD prototype used in the July 1990 beam tests.

Fig. 15 The angle and position resolution of the 180−straw TRD prototype. On average a pion crossed thirty straws.

Fig. 16 The energy spectrum measured in one straw, produced by one electron, one pion and two pions. The energy of the particles was 10 GeV. The three thresholds used for the cluster evaluation are also indicated.

Fig. 17 Number of clusters above a certain threshold produced by 10 GeV electrons and 3 (10) GeV pions in two radiators with different numbers of straws crossed, and at different angle between particle and crossed straw. The curve for 40 crossed straws is estimated by convoluting the signals from two particles.

Fig. 18 The γ−dependence of the probability to exceed an energy deposit E > 5 keV in a straw, for an electron efficiency of 90 %.

Fig. 19 a−e: Scatter plot of the probability for an energy deposit between TH_1 and TH_2 (N_{12}) vs the probability to exceed TH_3 (N_3). In Fig. 19a, the distribution is given for 30 GeV electrons; in Fig. 19b, for 10 GeV pions; in Figs 19c and 19d for 2 πs and 3 πs respectively; in Fig. 19e, the distribution for two overlapping electrons (e.g. from a conversion) is shown. The solid lines delineates the area for 90% electron efficiency. Mean value of crossed straws = 40.

Fig. 20 Measured pion rejection as a function of the π−momentum and the number of straws crossed.

Fig. 21 Display of a simulated event in a sector of the TRD−tracker, operated at $L = 2\times10^{34}$ cm^{-2} s^{-1}. In Fig. 21a all hits exceeding TH_1 are displayed. Hits above TH_3 are shown in Fig. 21b. The result of a tracking algorithm, requiring a sequence of energy depositions inside a 'road' consistent with an electron, is displayed in Fig. 21c.

Fig. 22 Scatterplot of the probability for an energy deposit between TH_1 and TH_2 (N_{12}) versus the probability to exceed TH_3 (N_3) in a multiplicity environment corresponding to $L = 2\times10^{34}$ cm^{-2} s^{-1}. The curves delineate the area for 90 % electron efficiency. Mean value of crossed straws = 40.
a. For reconstructed tracks produced by single electrons;
b. For reconstructed tracks produced by other particles including conversions and Dalitz decays.

Fig. 23 Monte Carlo–evaluated TRD rejection, of by the TRD reconstructed tracks, as a function of pseudorapidity and at various luminosities.

Fig. 24 a) reconstruction accuracy of the event vertex in the direction along the beam;
b) Accuracy, along the direction of the beam, of the reconstructed electron track extrapolated to the front face of the electromagnetic calorimeter.

Fig. 25 The rejection power against $\pi^{\pm}$, $K^{\pm}$, $p^{\pm}$ and γ, for 4 rapidity intervals. $E_T^{jet} > 100$ GeV, $L = 2 \times 10^{34}$ cm^{-2}s^{-1}.

Fig. 26 Rejection of isolated pions as a function of muon energy, for criteria that give 90% muon efficiency, demonstrating the 'muon–tagging' capability of the proposed TRD–tracker.

Fig. 27 Conceptual functional diagram of the readout and trigger architecture for the TRD–tracker.

Fig. 28 Cross–section through the halo detector showing possible dimensions of straw and foam layers.

Fig. 29 Conceptual construction of multi–straws using pressure–formed aluminium–cladded Mylar foils. The foam radiator provides the mechanical backing for the foils.

Fig. 30 Layout of the 32–channel Mach–Zender interferometer used to modulate light with the straw–tube signal. Light at 1.3 μm wavelength is piped into the device through a polarization–preserving fibre. Bonding pads are used to couple the electrical signal from the straw tubes into the interferometer. There are 32 output fibres, one per channel; they are attached to the interferometers with a snap–on connector, aligned through a V–groove silicon–fibre aligner.

Table 1: ASIC Developments Relevant for the TRD Frontend

Design purpose	Drift chamber readout[a)]	Si or MWPC readout[b)]	Si or MWPC readout[c)]	Fast RICH[d)]
Peaking time	8 ns	15 ns	8 ns	5 ns
r.m.s. noise	1000 e	1000 e	1000 e	1000 e
Power consumpt.	5 mW	2 mW	~ 3 mW	10 mW
Technology	Bipolar	3 μm CMOS lateral bipolar transistor	1.5 μm CMOS	Bipolar
Channels per Chip	4	4	8	8
Availability	Prototypes under test	Existing	Prototypes in July 1990	Prototypes in July 1990

a) H.H. Williams et al., 'Frontend electronics development for SSC detectors', (1990)
b) F. Anghinolfi et al., 'Development of integrated CMOS circuits and Si pixel detector in the CERN LAA project', CERN/EF 89–14, CERN/LAA SD 89–11, 13th September 1989, p. 10.
c) P. Jarron et al., work in progress, CERN
d) M. French et al., Rutherfor lab. reports, RAL–110, RAL–111.

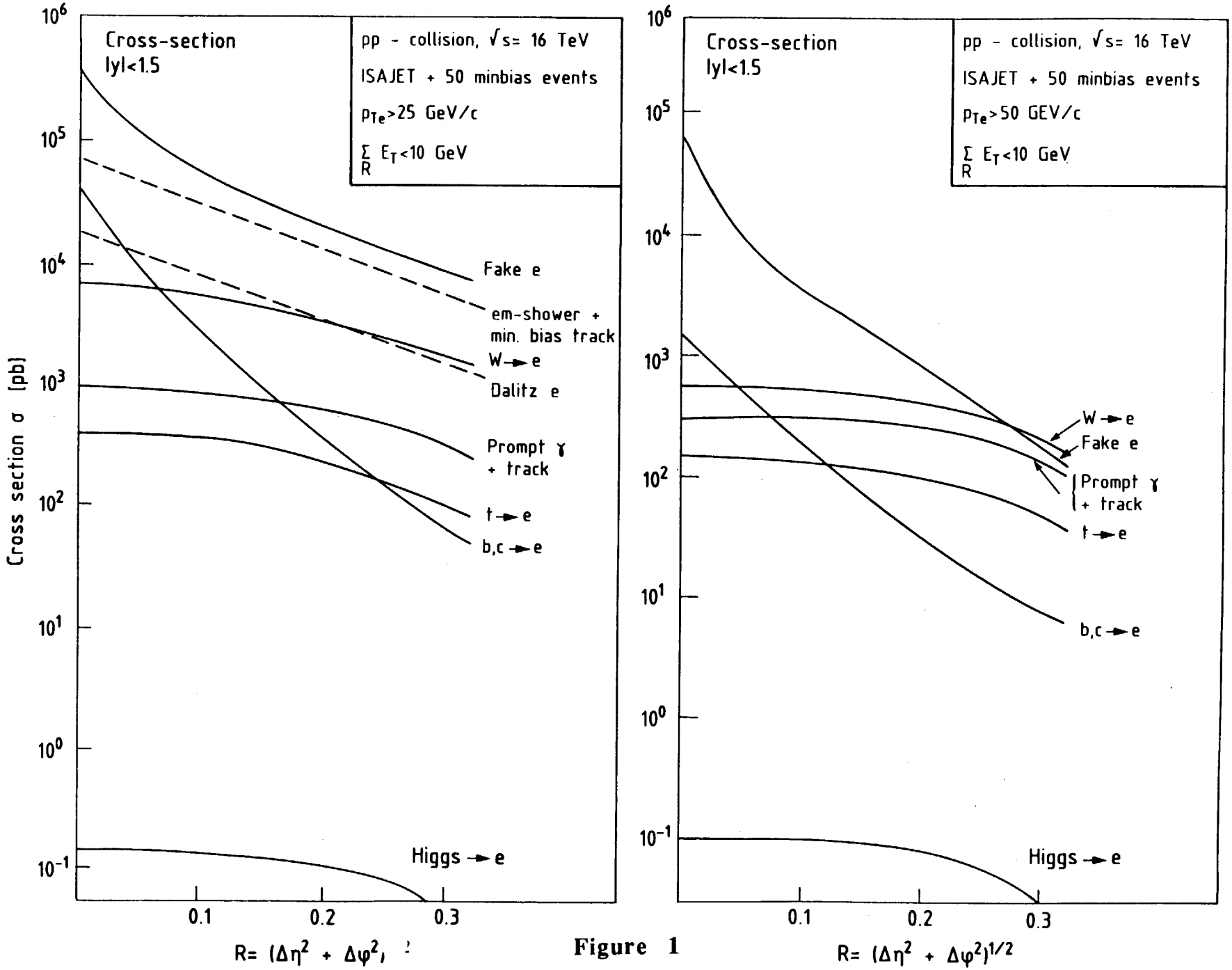
Cross-section
|y|<1.5
pp - collision, √s= 16 TeV
ISAJET + 50 minbias events
p_{Te}>25 GeV/c
$\sum_R E_T$<10 GeV
Fake e
em-shower + min. bias track
W→e
Dalitz e
Prompt γ + track
t→e
b,c→e
Higgs→e
Cross section σ [pb]
$R= (\Delta\eta^2 + \Delta\varphi^2)$
Cross-section
|y|<1.5
pp - collision, √s= 16 TeV
ISAJET + 50 minbias events
p_{Te}>50 GEV/c
$\sum_R E_T$<10 GeV
W→e
Fake e
Prompt γ + track
t→e
b,c→e
Higgs→e
$R= (\Delta\eta^2 + \Delta\varphi^2)^{1/2}$

Figure 1

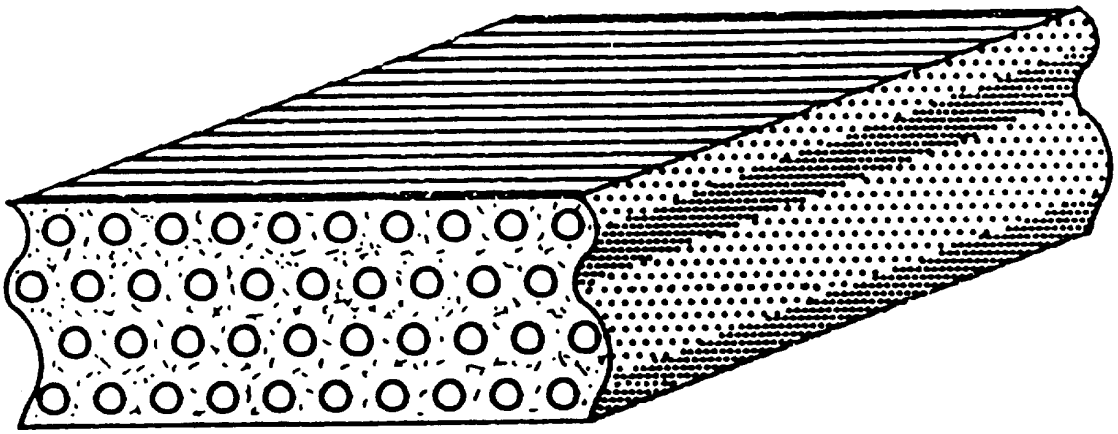

Figure 2

Plan de Mesure

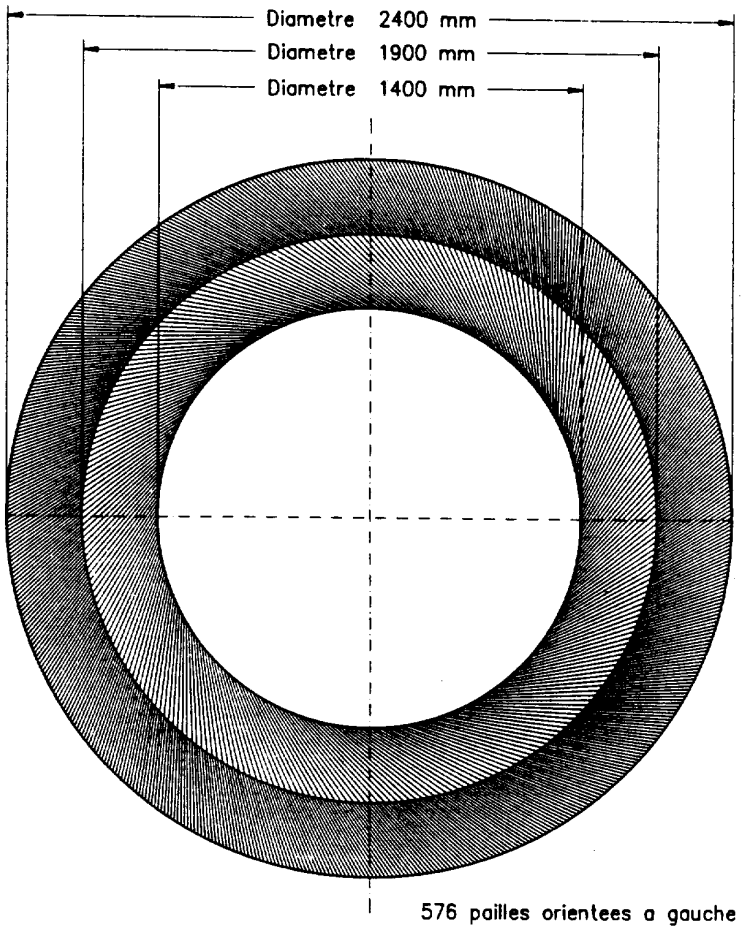

Experience HALO

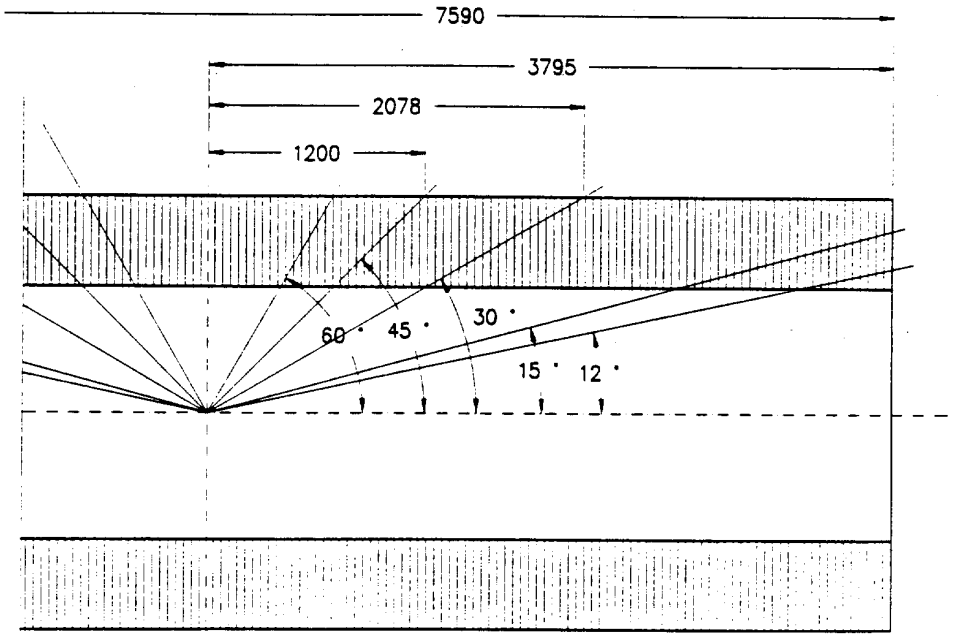

Experience HALO Angles

Figure 3

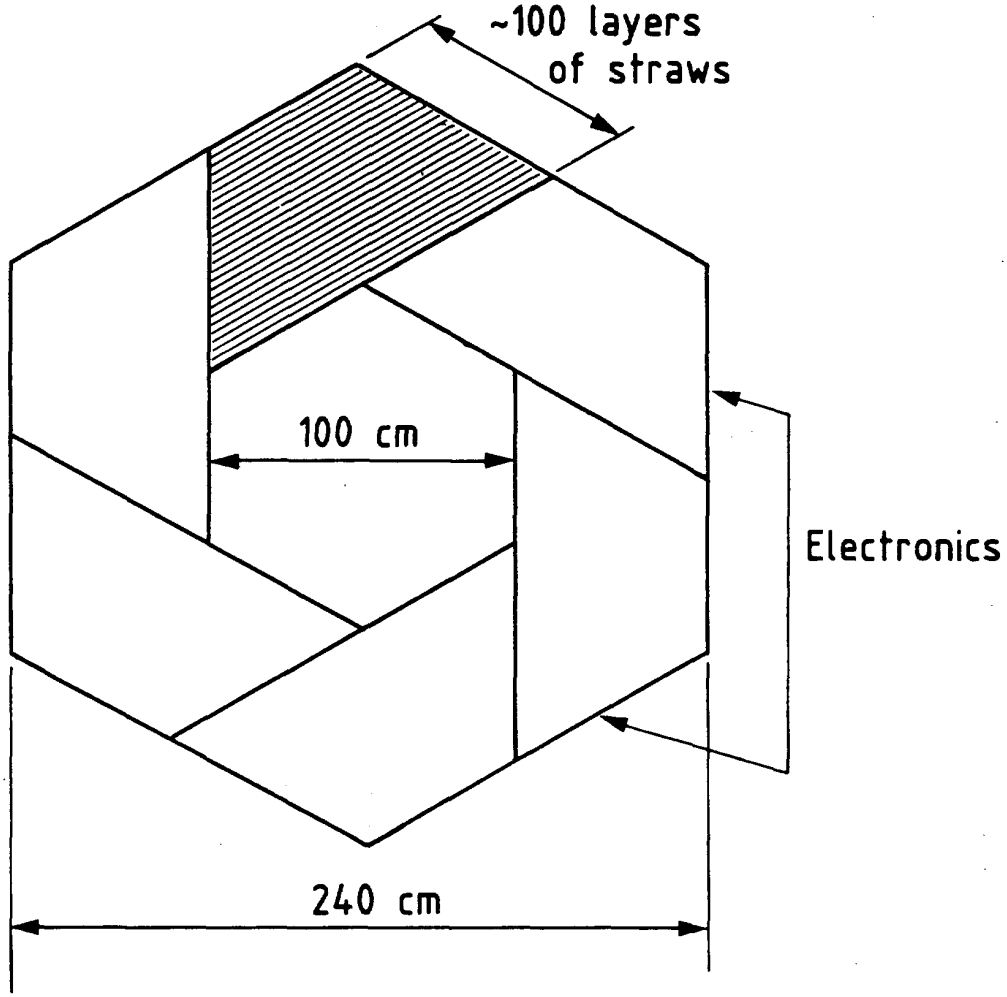

Figure 4

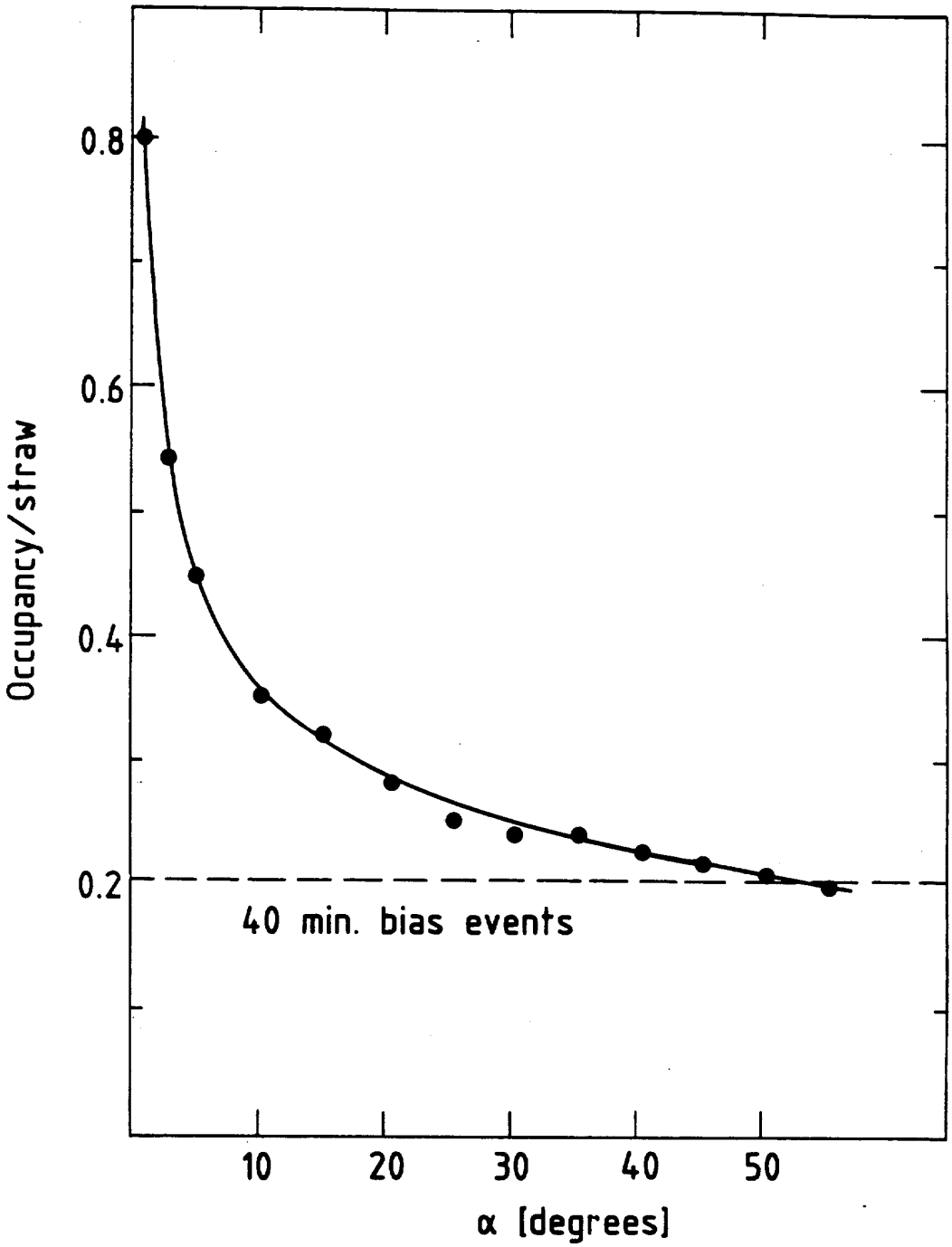
0.8
0.6
0.4
0.2
Occupancy/straw
40 min. bias events
10
20
30
40
50
α [degrees]

Figure 5

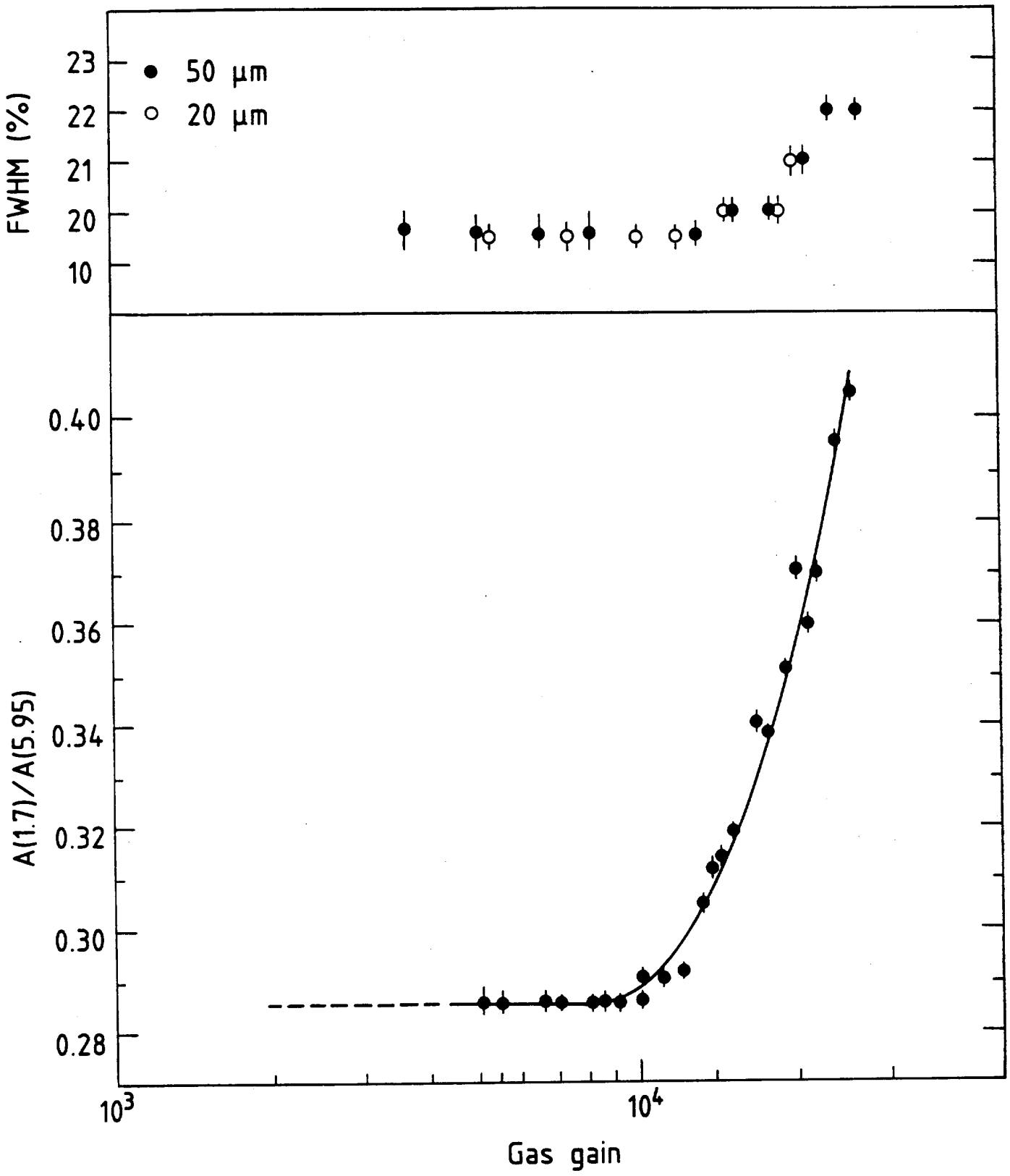
FWHM (%)
23
22
21
20
10
50 µm
20 µm
A(1.7)/A(5.95)
0.40
0.38
0.36
0.34
0.32
0.30
0.28
10^3
10^4
Gas gain

Figure 6

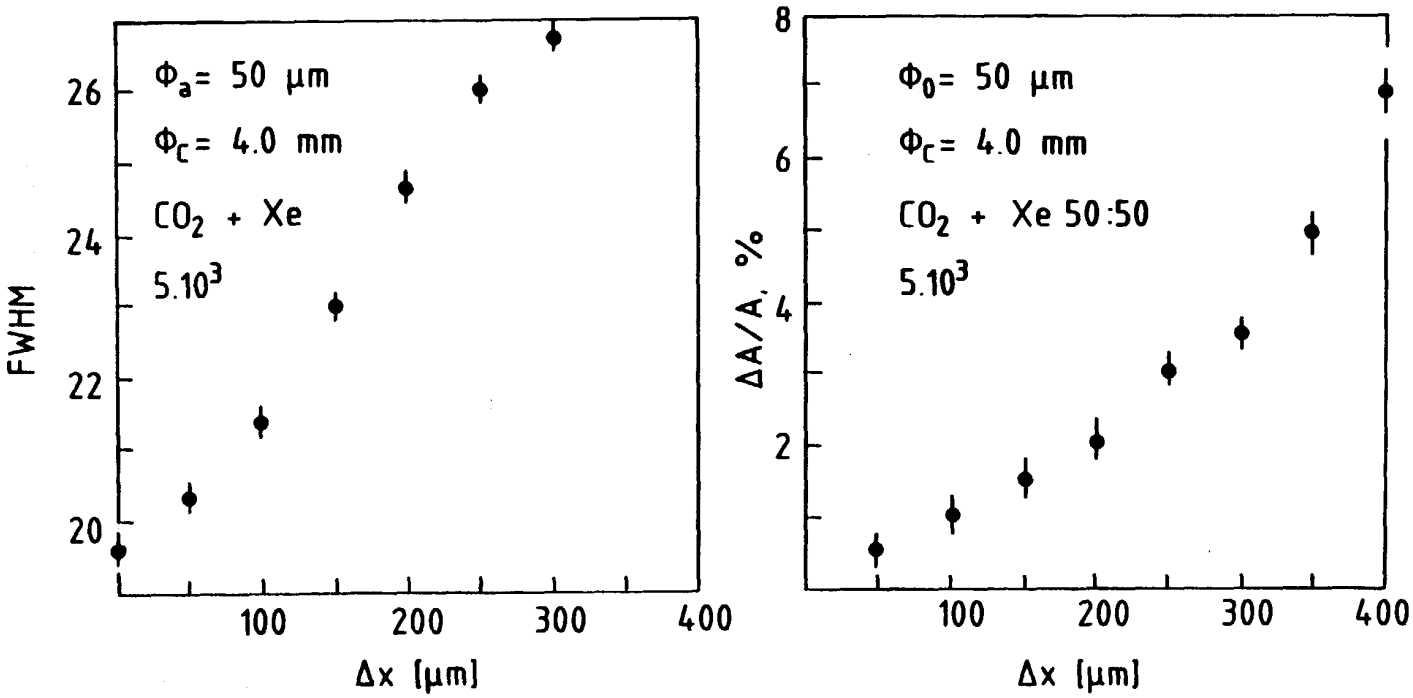
FWHM
26
24
22
20
100
200
300
400
Δx [μm]
Φa= 50 μm
Φc= 4.0 mm
CO2 + Xe
5.10^3
ΔA/A, %
8
6
4
2
100
200
300
400
Δx [μm]
Φ0= 50 μm
Φc= 4.0 mm
CO2 + Xe 50:50
5.10^3

Figure 7

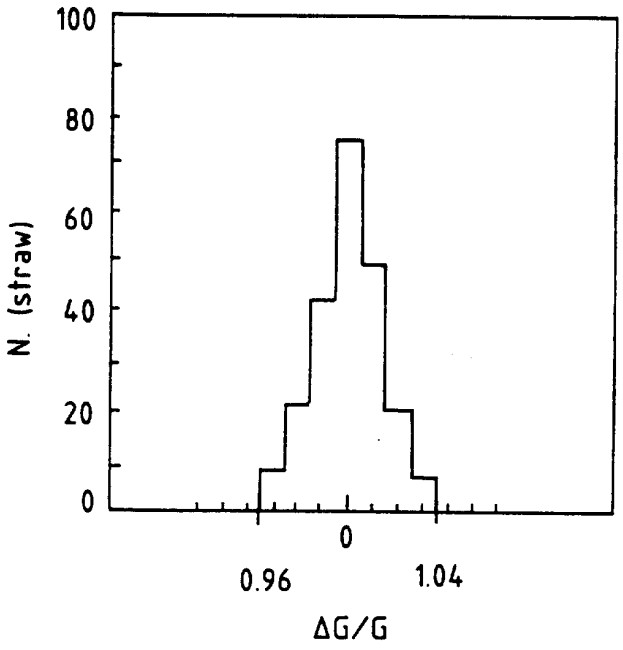

Figure 8

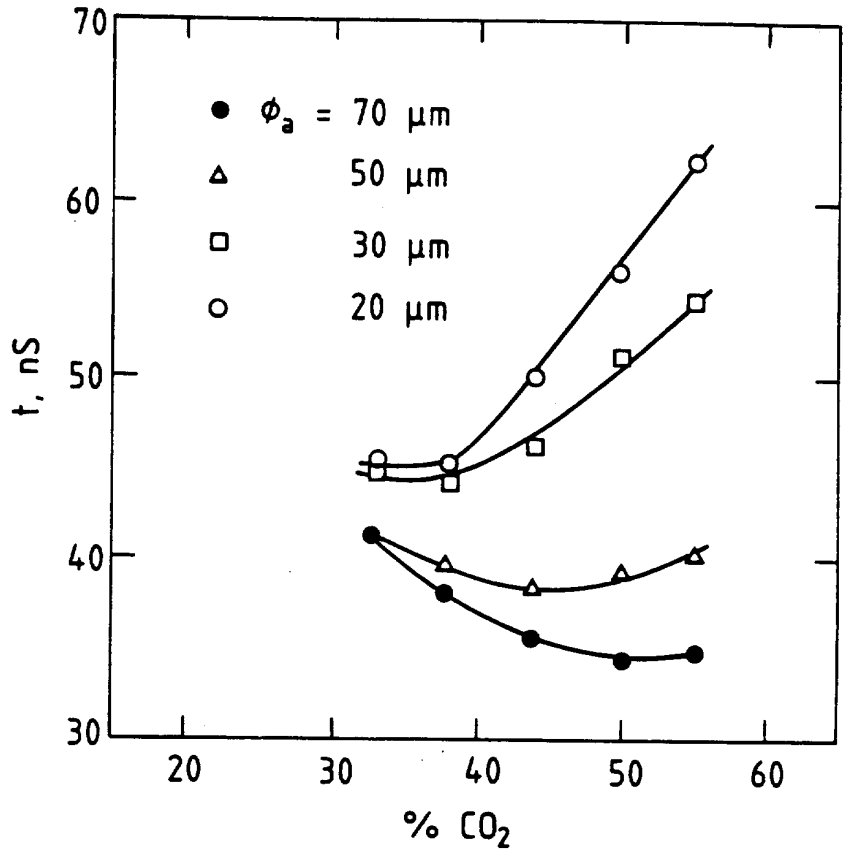

Figure 9

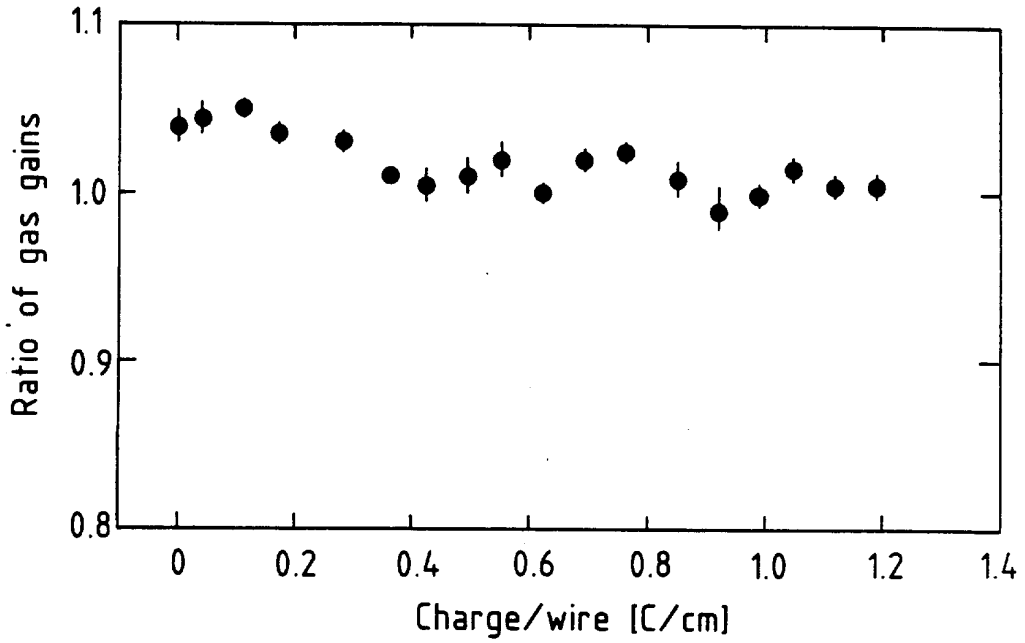
1.1
1.0
0.9
0.8
Ratio of gas gains
0
0.2
0.4
0.6
0.8
1.0
1.2
1.4
Charge/wire [C/cm]

Figure 10

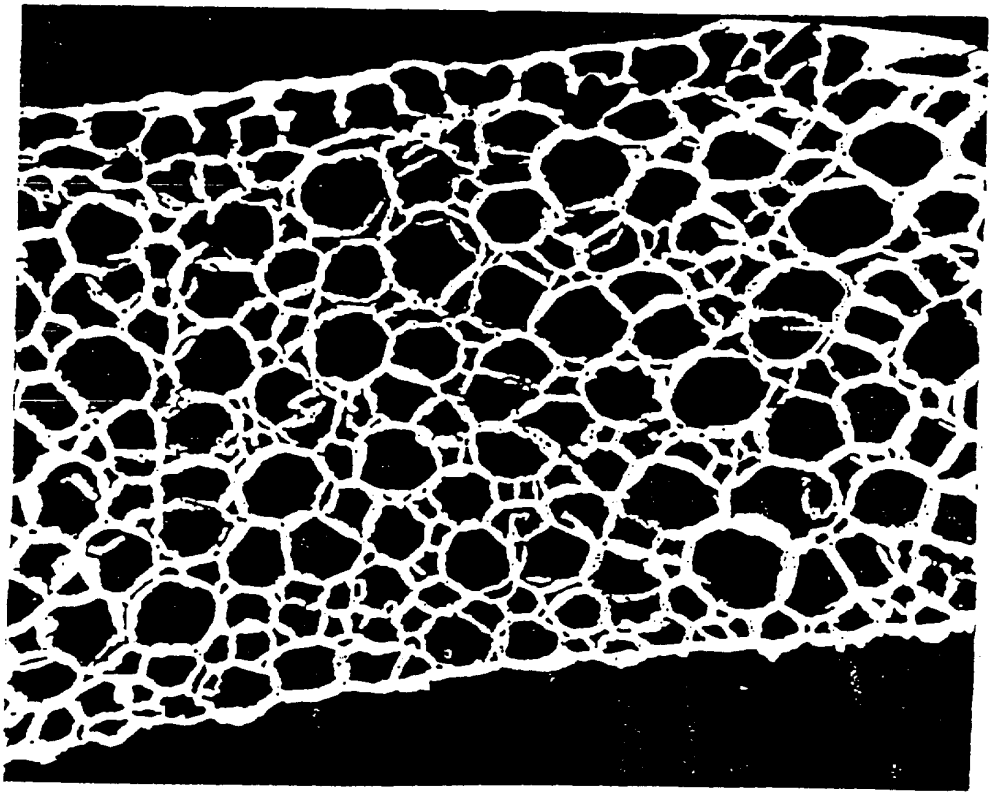

Figure 11

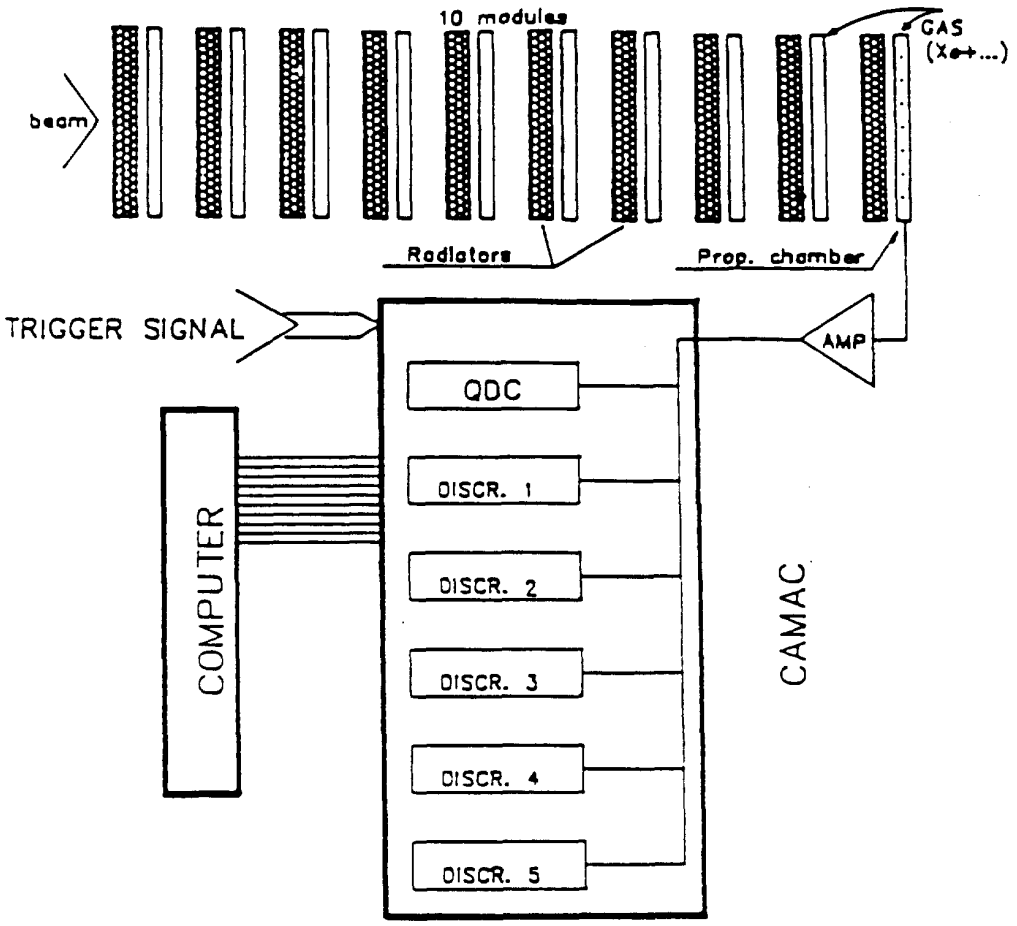
10 modules
GAS
(Xe+...)
beam
Radiators
Prop. chamber
TRIGGER SIGNAL
AMP
QDC
DISCR. 1
DISCR. 2
DISCR. 3
DISCR. 4
DISCR. 5
COMPUTER
CAMAC

Figure 12

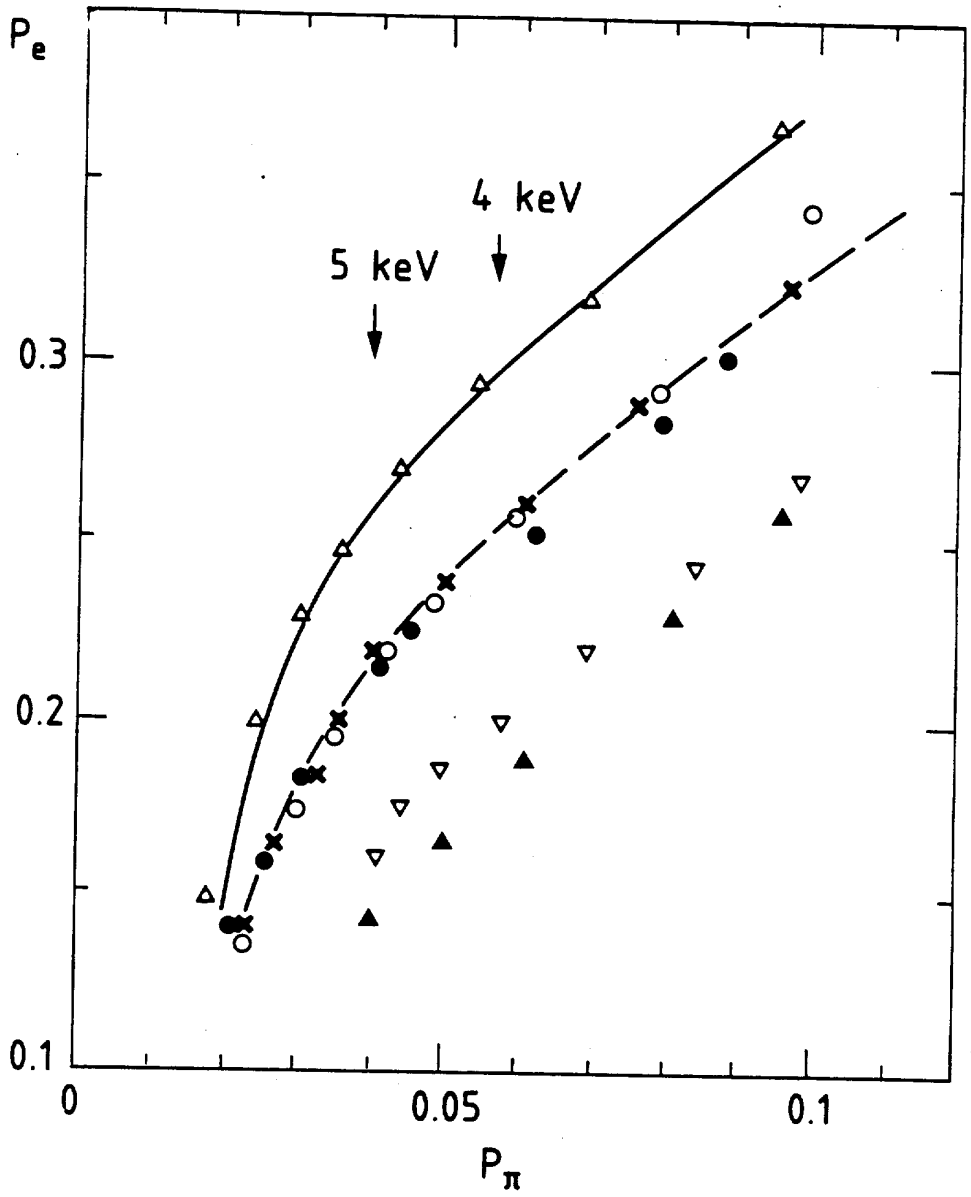

Figure 13

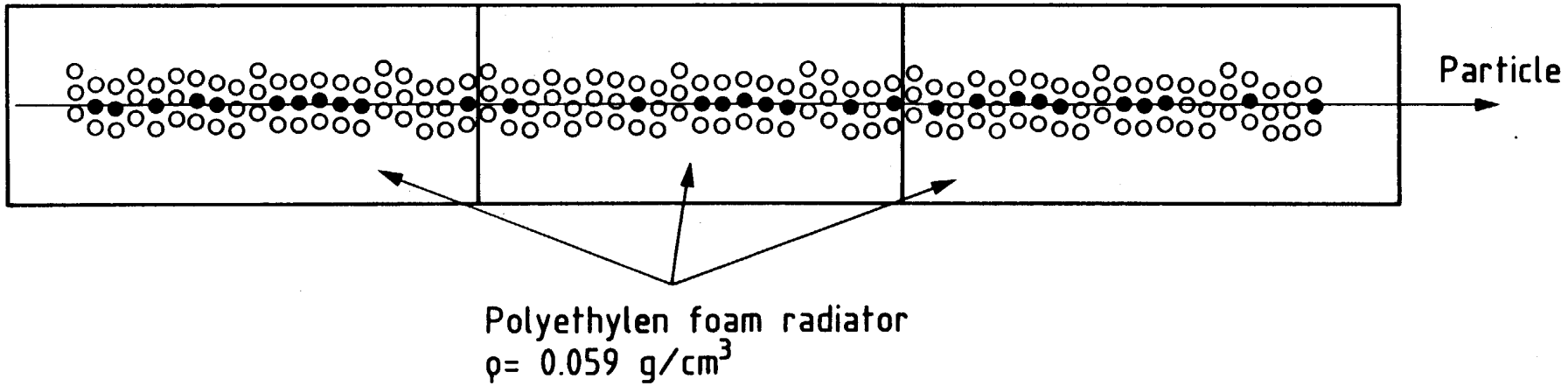

Figure 14

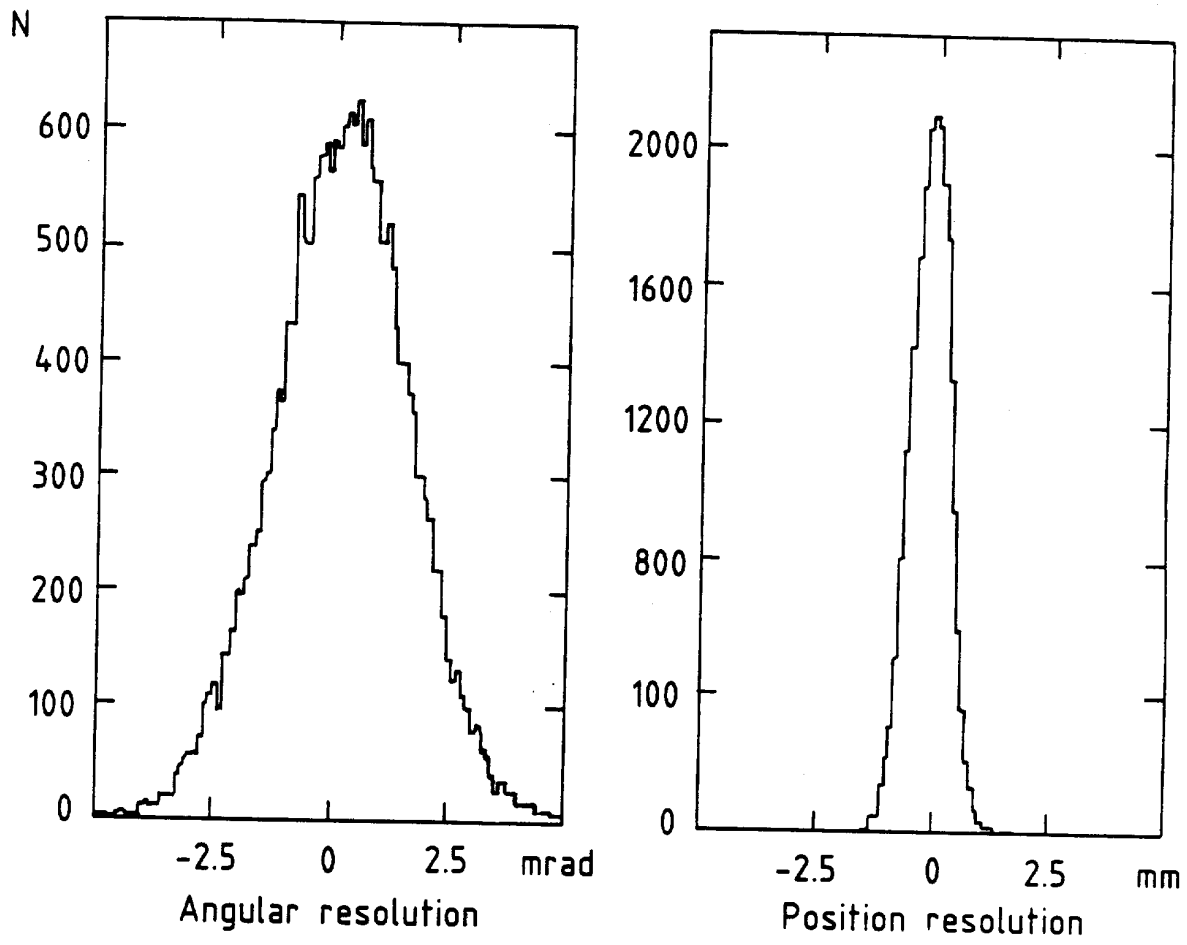
N
600
500
400
300
200
100
0
-2.5
0
2.5
mrad
Angular resolution
2000
1600
1200
800
100
0
-2.5
0
2.5
mm
Position resolution

Figure 15

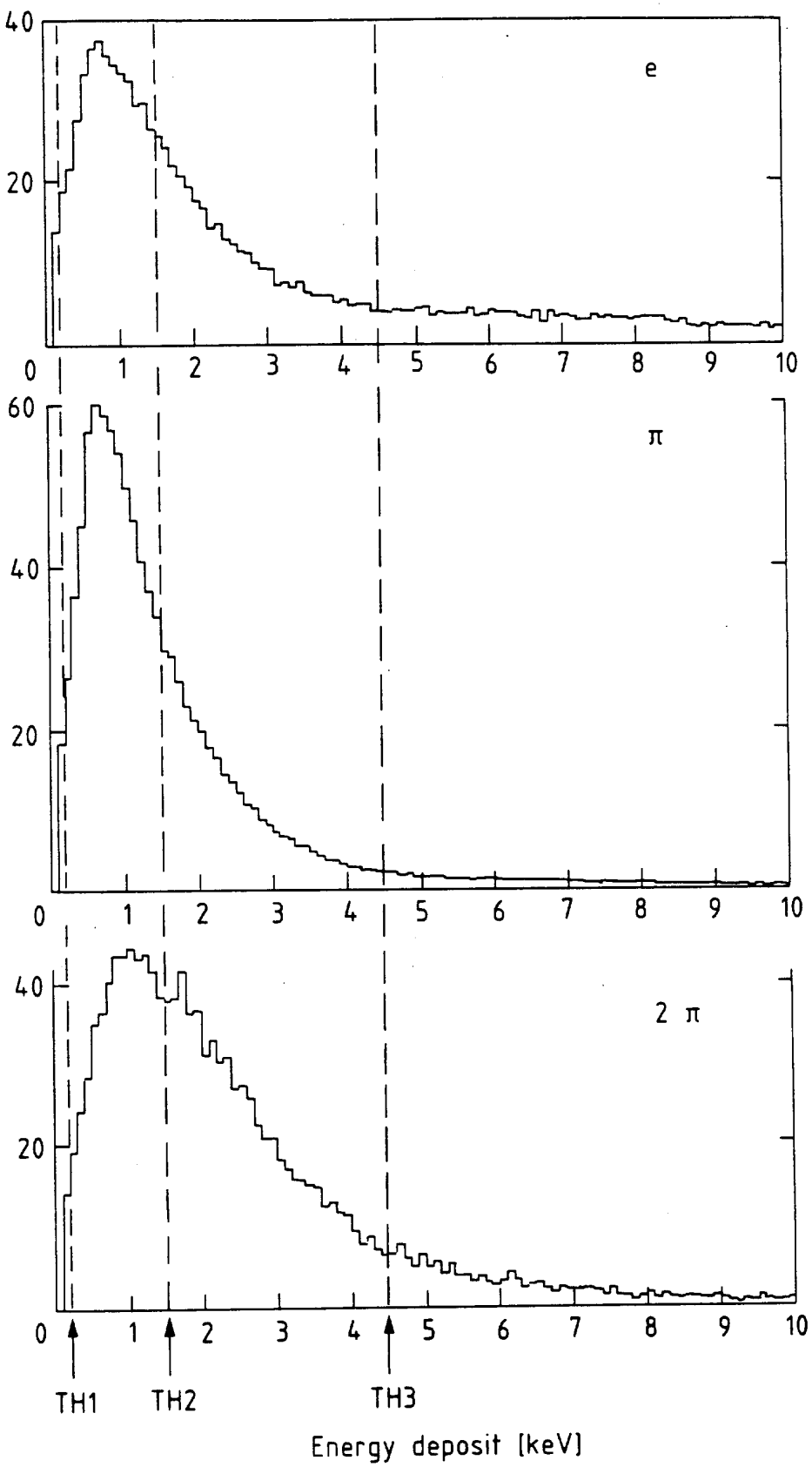

Figure 16

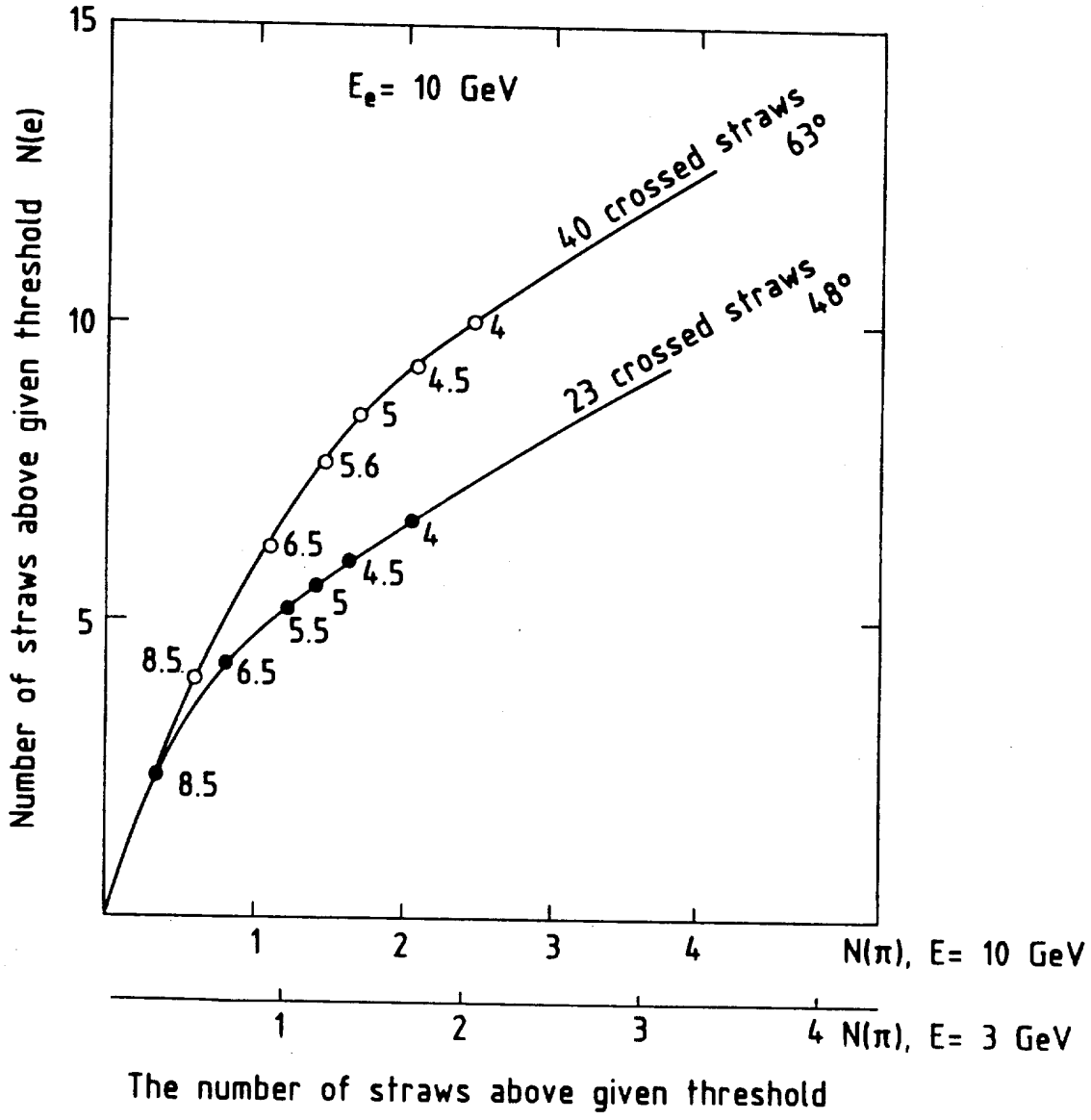
15
10
5
E_e= 10 GeV
40 crossed straws
63°
23 crossed straws
48°
4
4.5
5
5.6
6.5
8.5
4
4.5
5
5.5
6.5
8.5
Number of straws above given threshold N(e)
1
2
3
4
N(π), E= 10 GeV
1
2
3
4 N(π), E= 3 GeV
The number of straws above given threshold

Figure 17

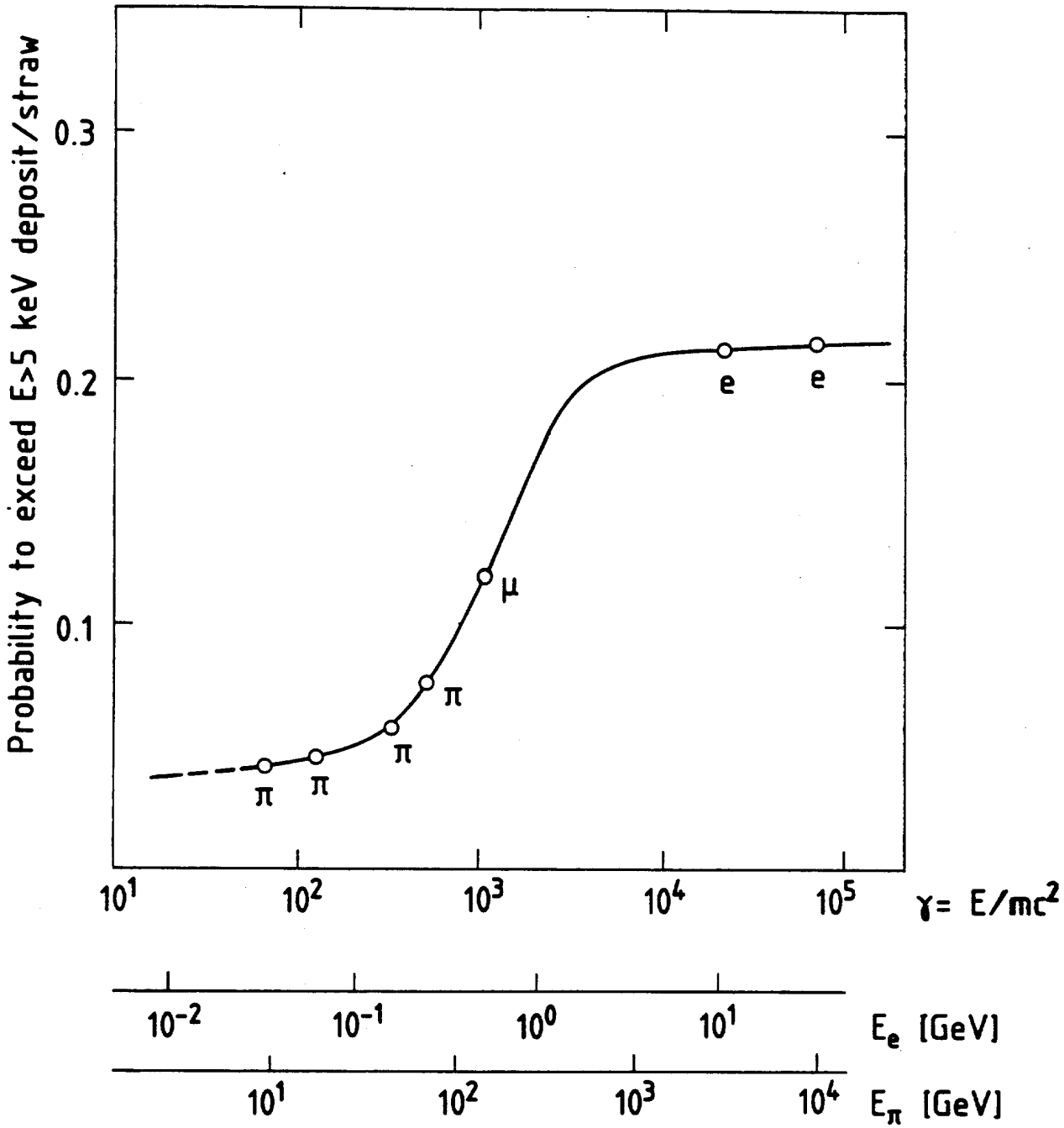
Probability to exceed E>5 keV deposit/straw
0.3
0.2
0.1
π
π
π
π
μ
e
e
10¹
10²
10³
10⁴
10⁵
γ= E/mc²
10⁻²
10⁻¹
10⁰
10¹
E_e [GeV]
10¹
10²
10³
10⁴
E_π [GeV]

Figure 18

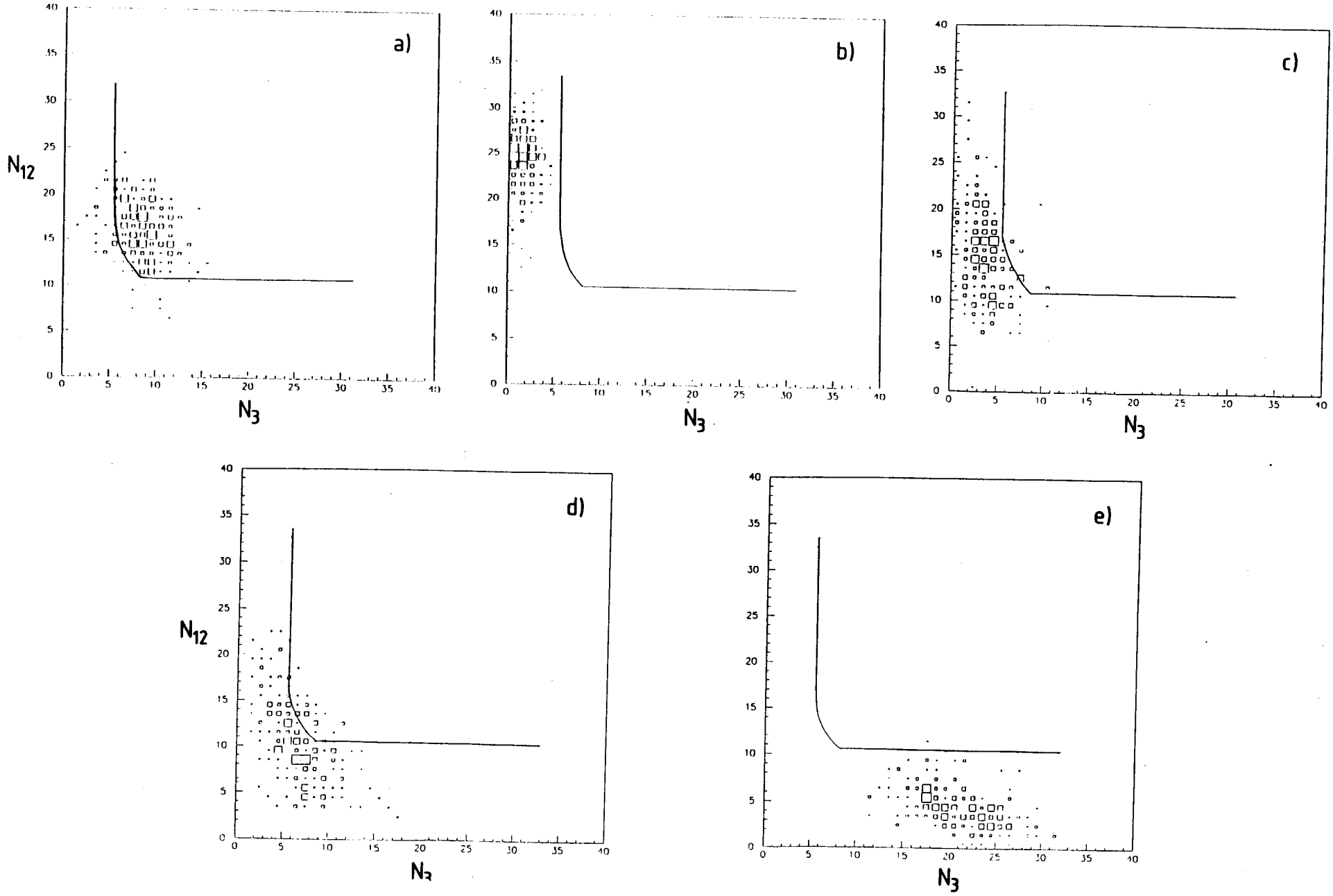

Figure 19

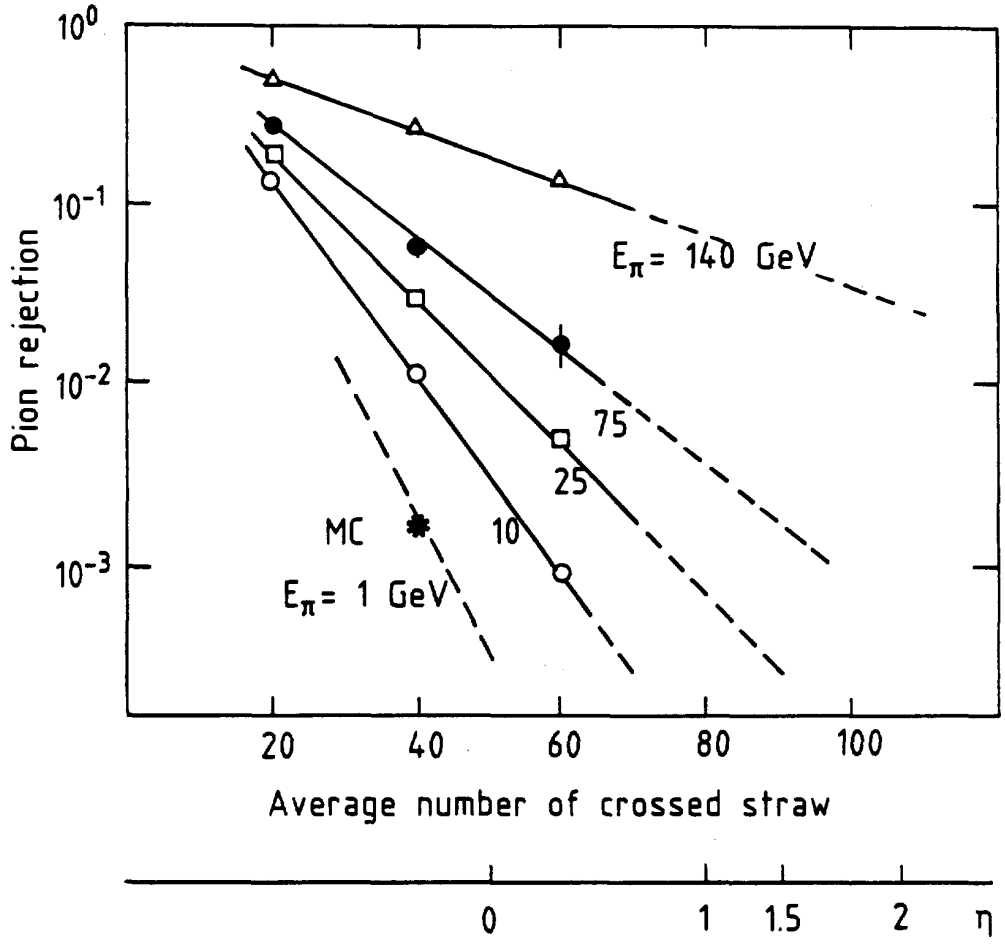
10^0
10^{-1}
10^{-2}
10^{-3}
Pion rejection
E_π= 140 GeV
75
25
10
MC
E_π= 1 GeV
20
40
60
80
100
Average number of crossed straw
0
1
1.5
2
η

Figure 20

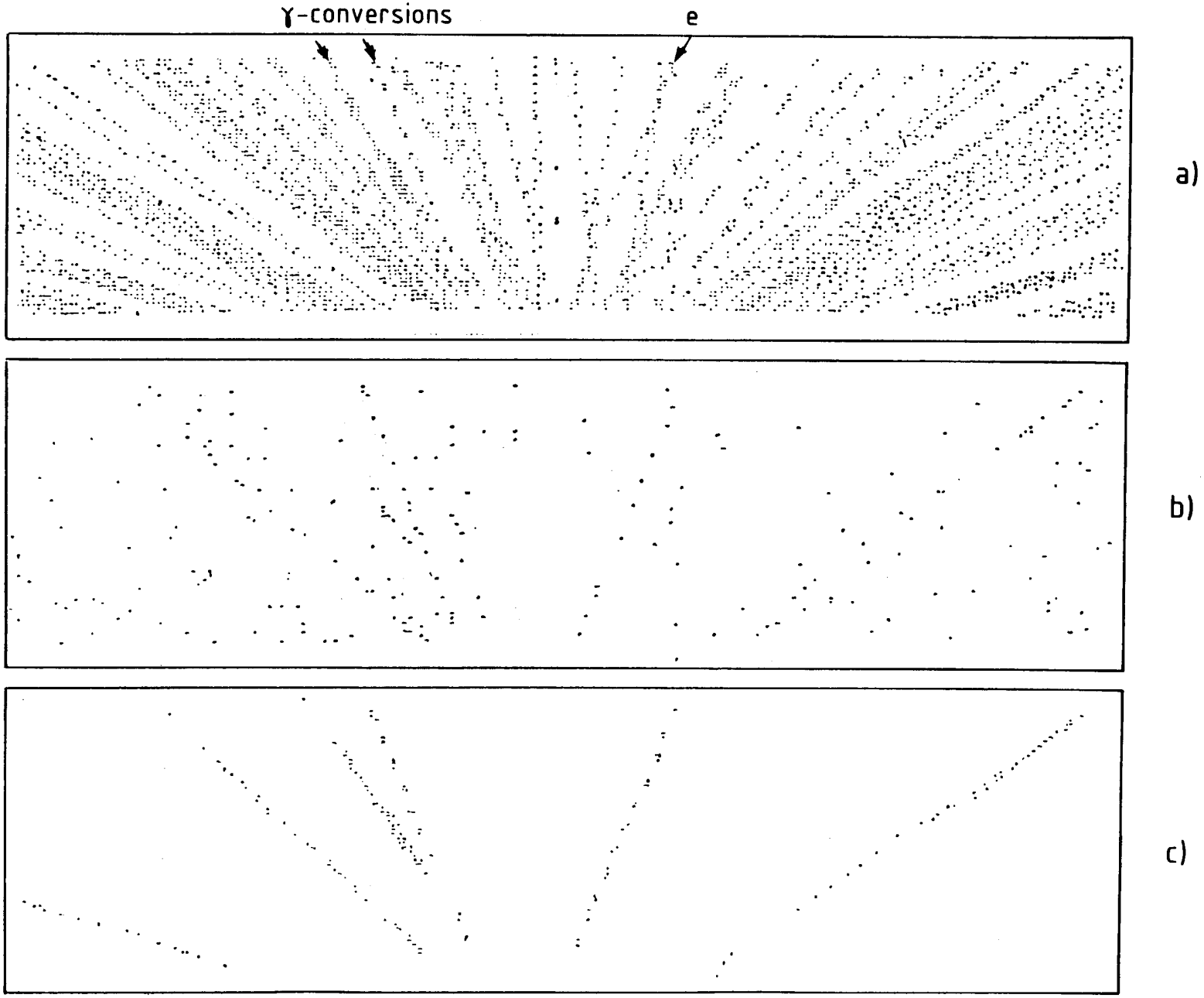

Figure 21

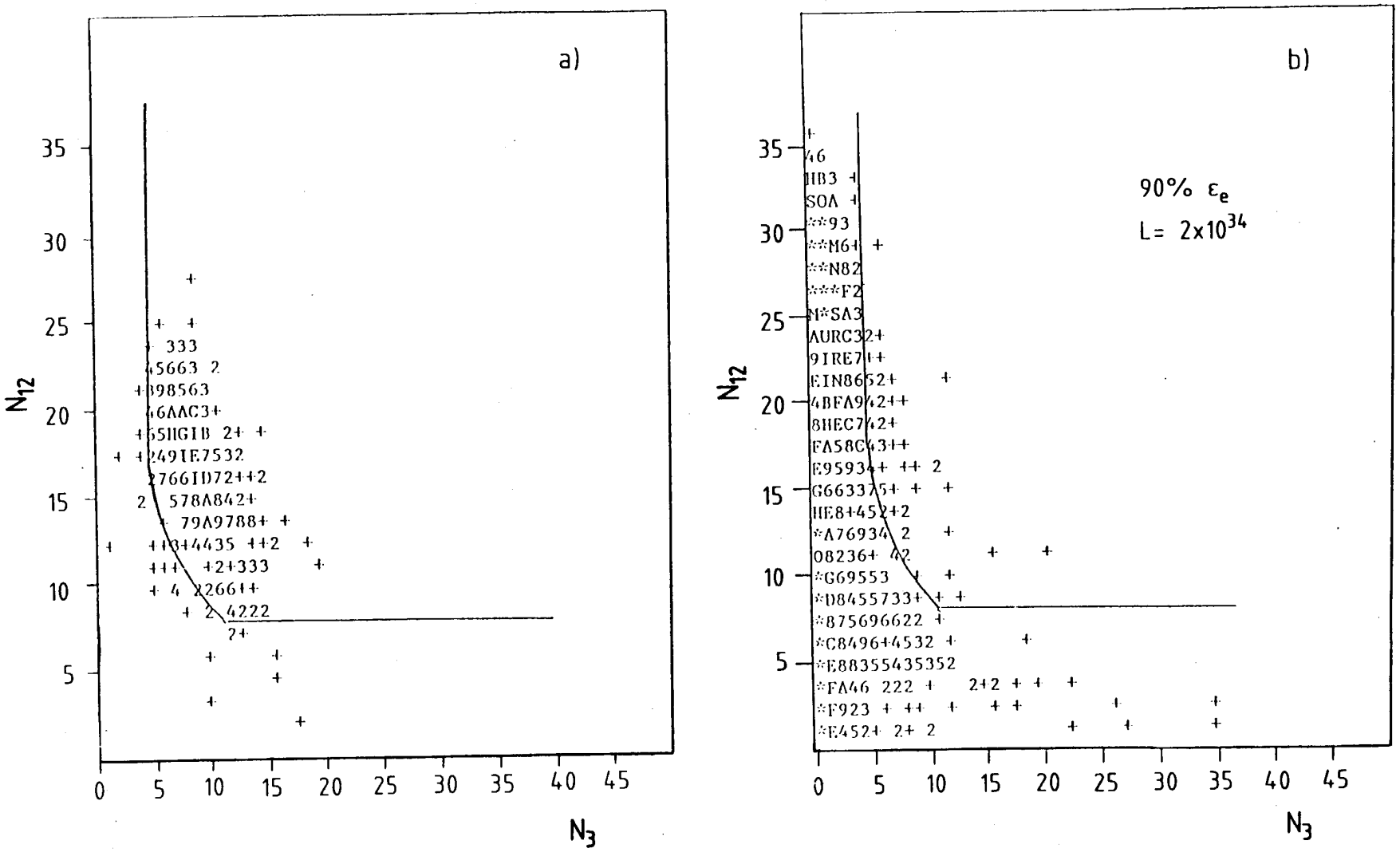

Figure 22

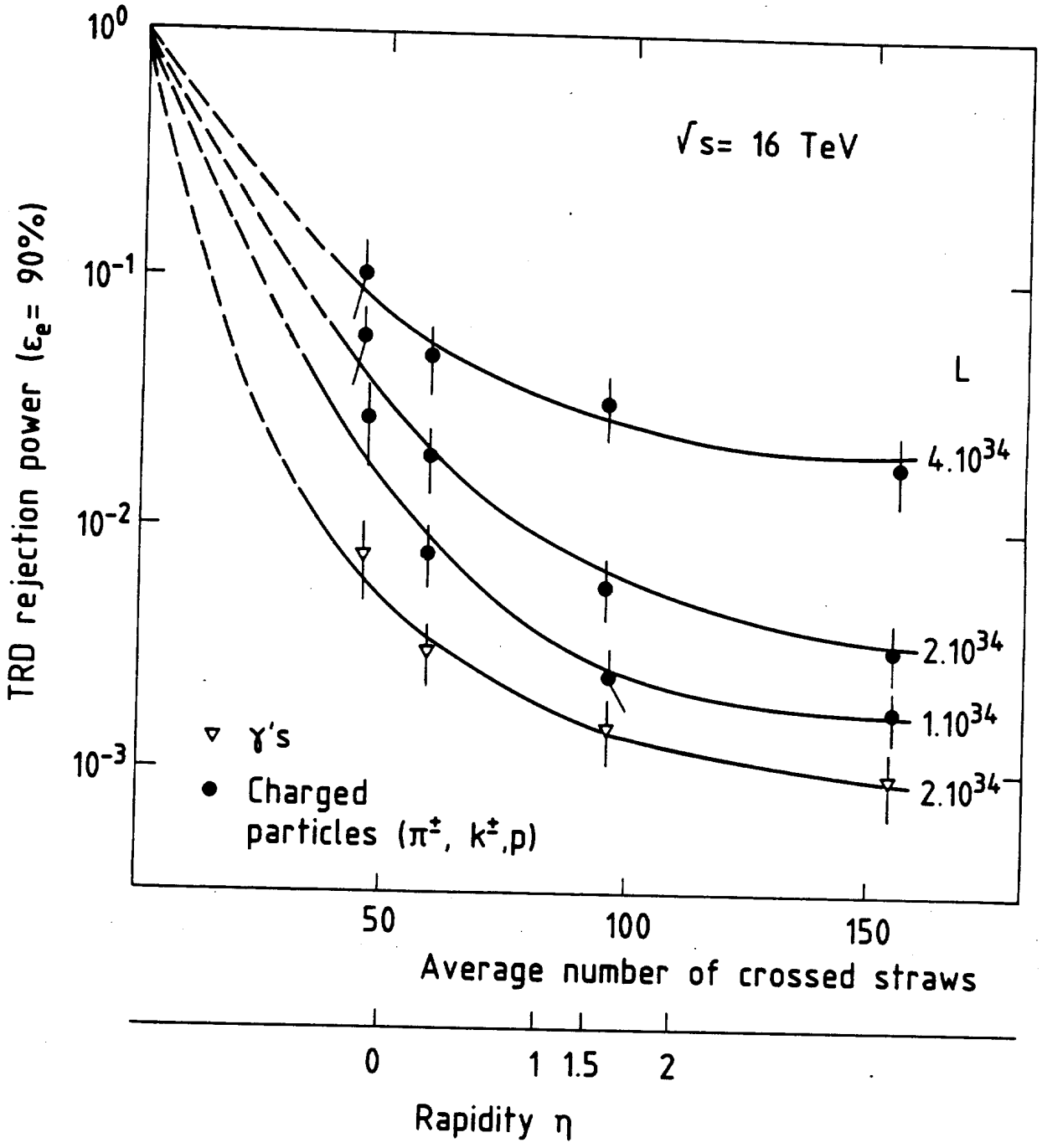
10^0
10^{-1}
10^{-2}
10^{-3}
TRD rejection power (ε_e= 90%)
$\sqrt{s}$= 16 TeV
L
4.10^{34}
2.10^{34}
1.10^{34}
2.10^{34}
γ's
Charged particles ($\pi^{\pm}$, $k^{\pm}$,p)
50
100
150
Average number of crossed straws
0
1
1.5
2
Rapidity η

Figure 23

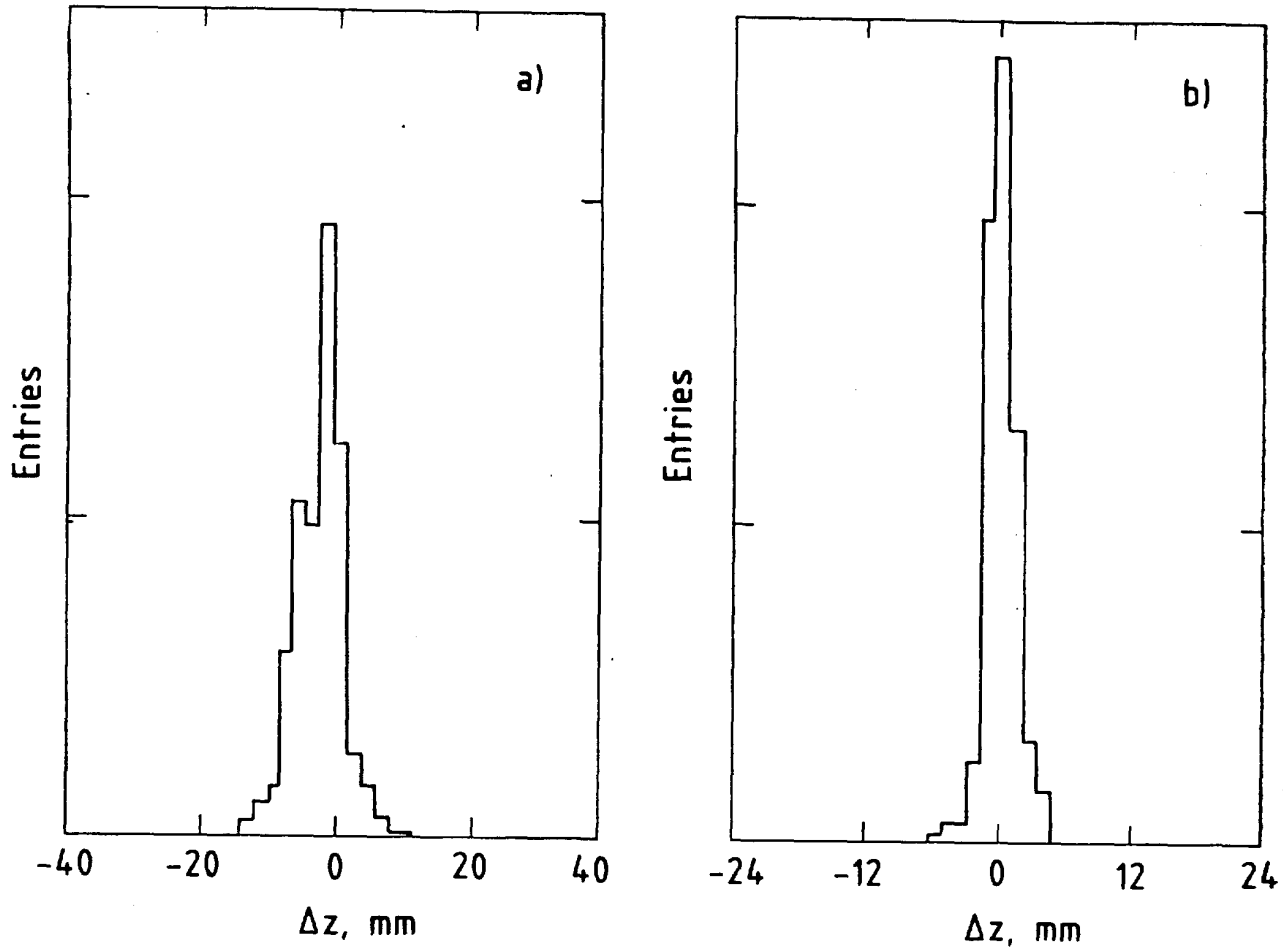

Figure 24

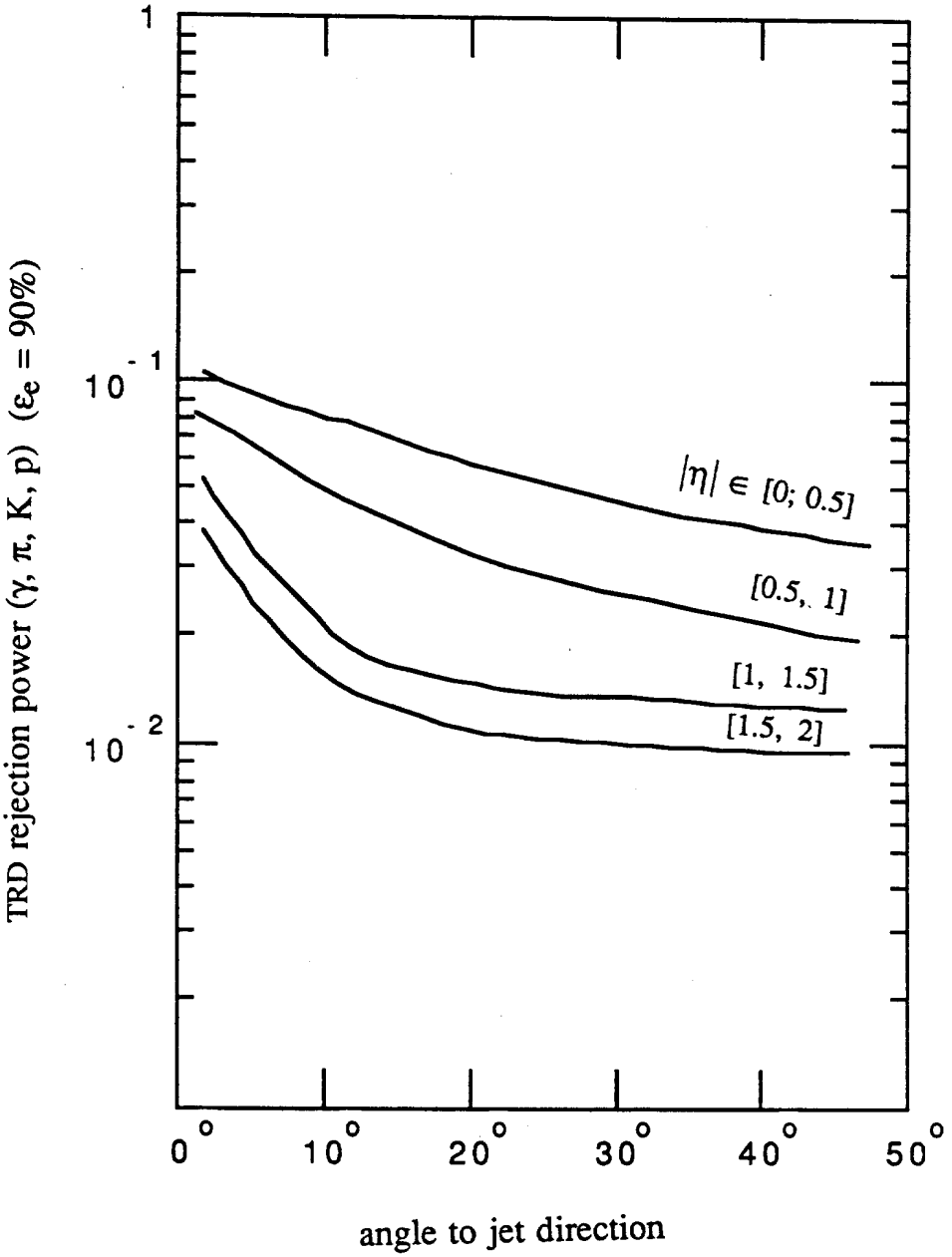
1
10^{-1}
10^{-2}
TRD rejection power (γ, π, K, p) (ε_e = 90%)
$|\eta| \in [0; 0.5]$
[0.5, 1]
[1, 1.5]
[1.5, 2]
0°
10°
20°
30°
40°
50°
angle to jet direction

Figure 25

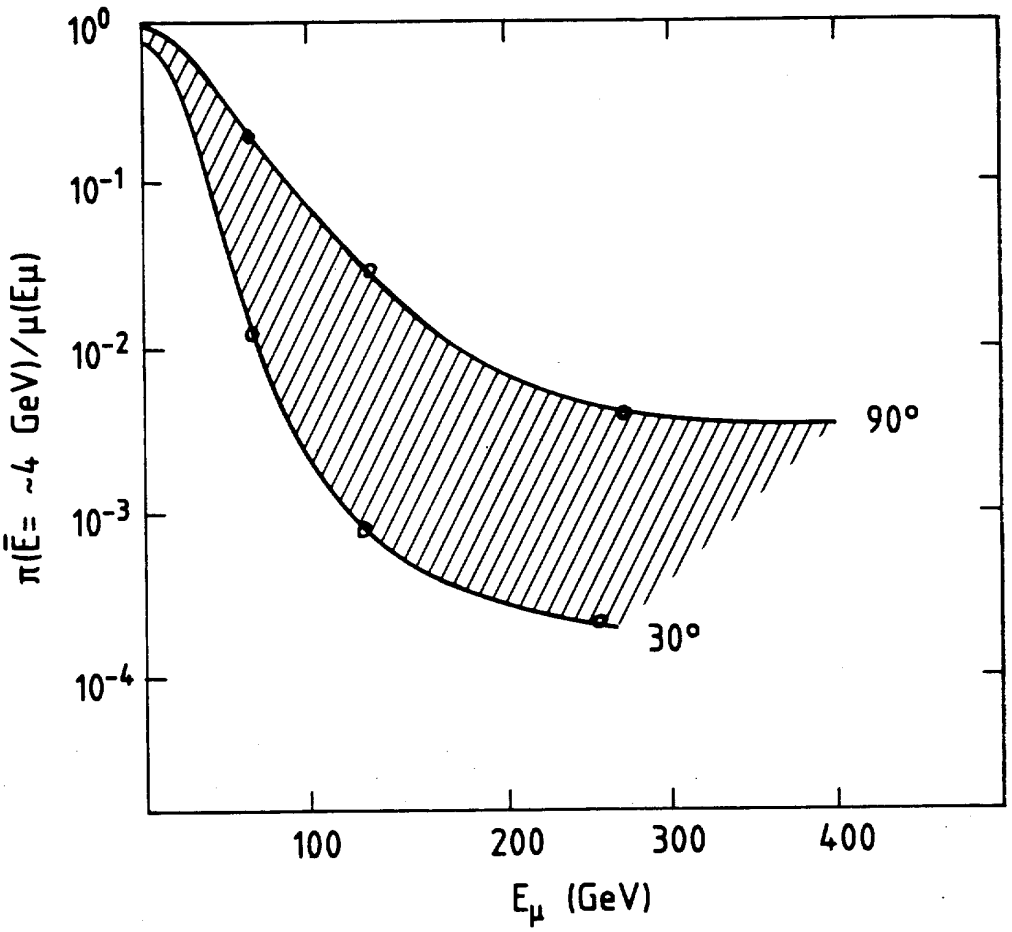
10^0
10^{-1}
10^{-2}
10^{-3}
10^{-4}
$\pi(\bar{E}= \sim 4$ GeV)/$\mu(E\mu)$
90°
30°
100
200
300
400
E_μ (GeV)

Figure 26

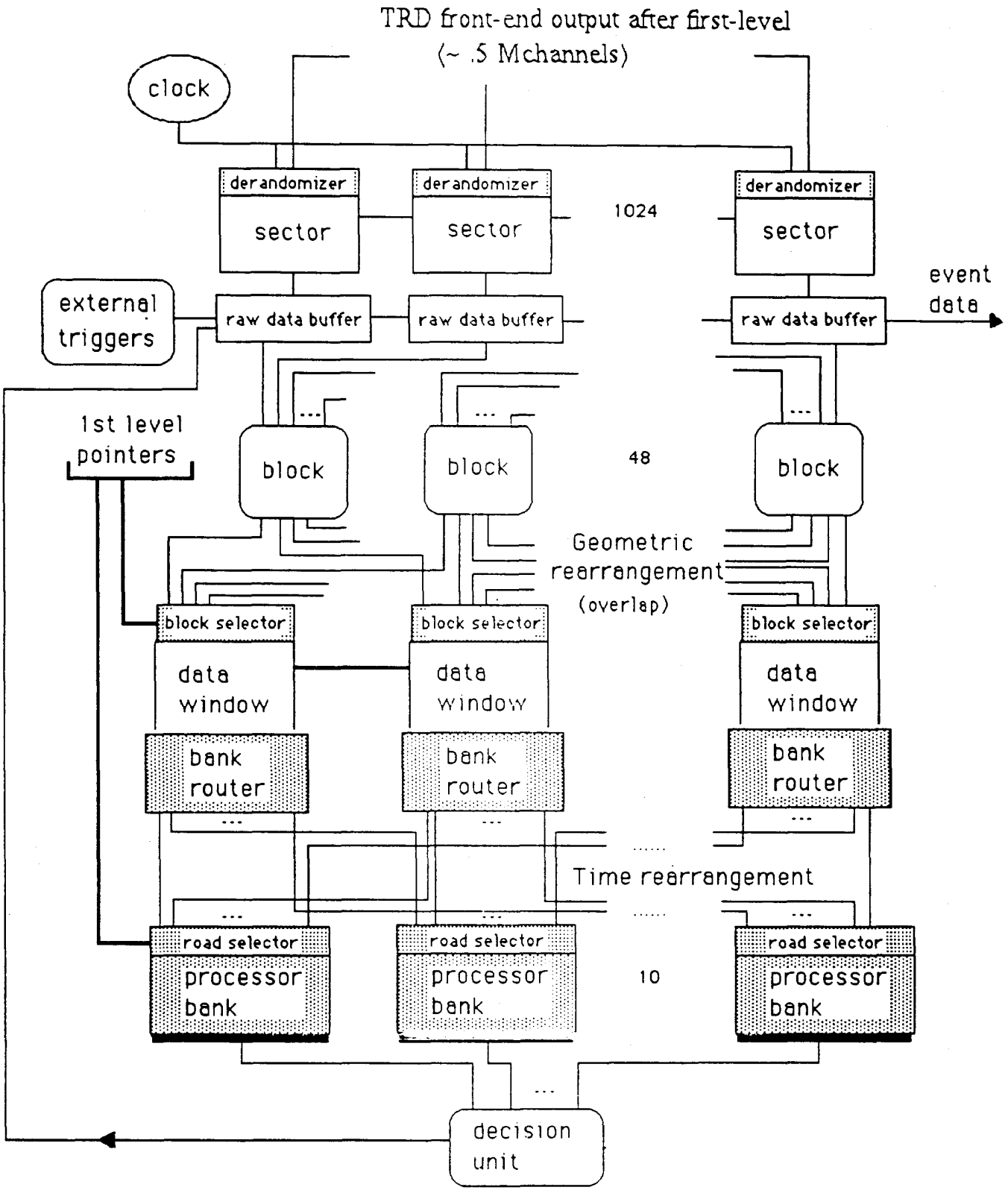
TRD front-end output after first-level
(~ .5 Mchannels)
clock
derandomizer
sector
derandomizer
sector
1024
derandomizer
sector
event
data
external
triggers
raw data buffer
raw data buffer
raw data buffer
1st level
pointers
block
block
48
block
Geometric
rearrangement
(overlap)
block selector
block selector
block selector
data
window
data
window
data
window
bank
router
bank
router
bank
router
Time rearrangement
road selector
processor
bank
road selector
processor
bank
10
road selector
processor
bank
decision
unit

Figure 27

Traces dans le plan a 90 °

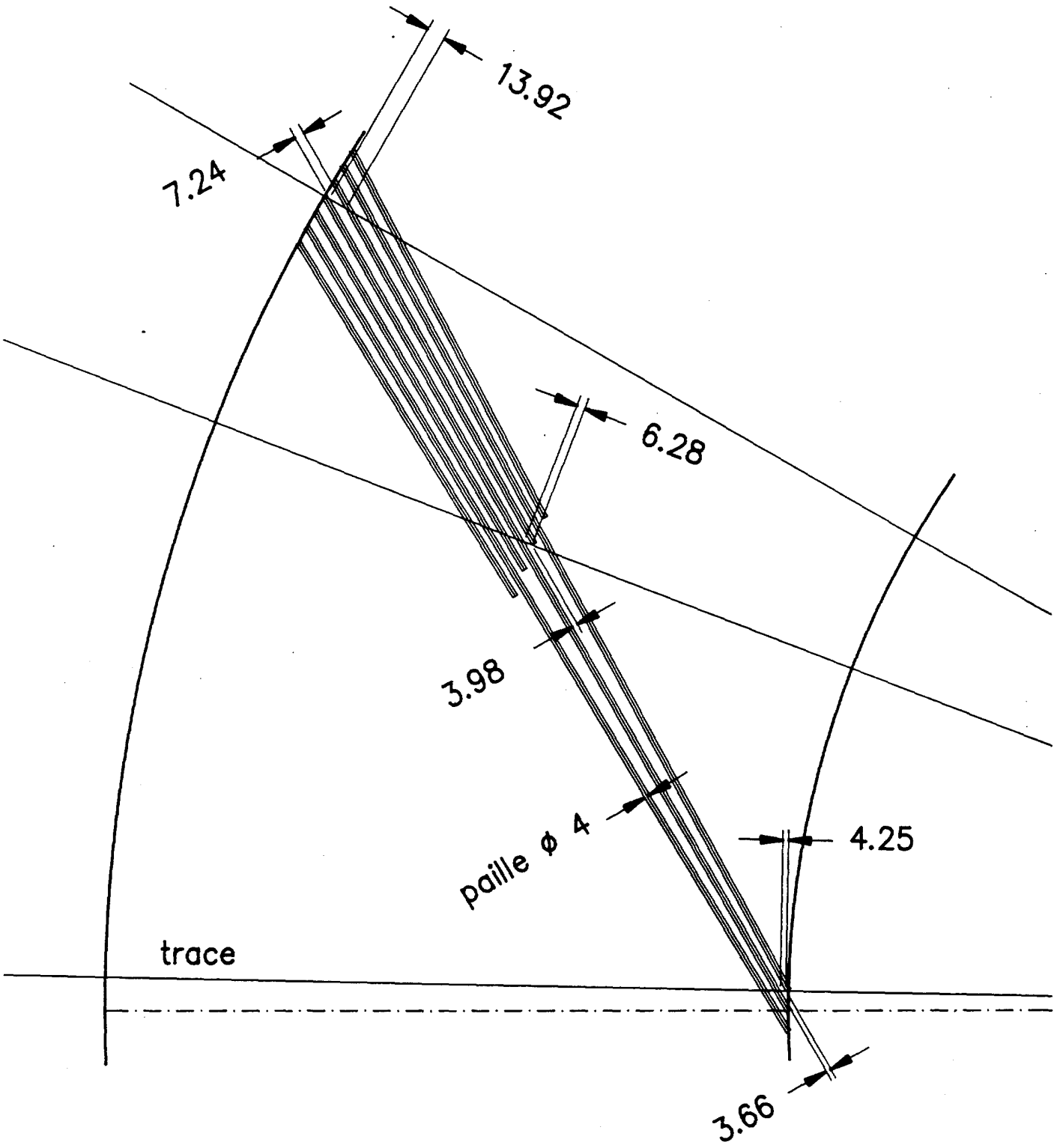

Experience HALO

Figure 28

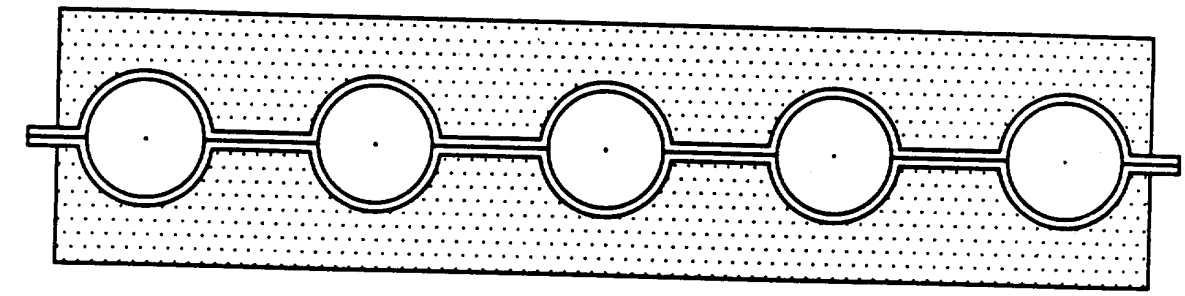

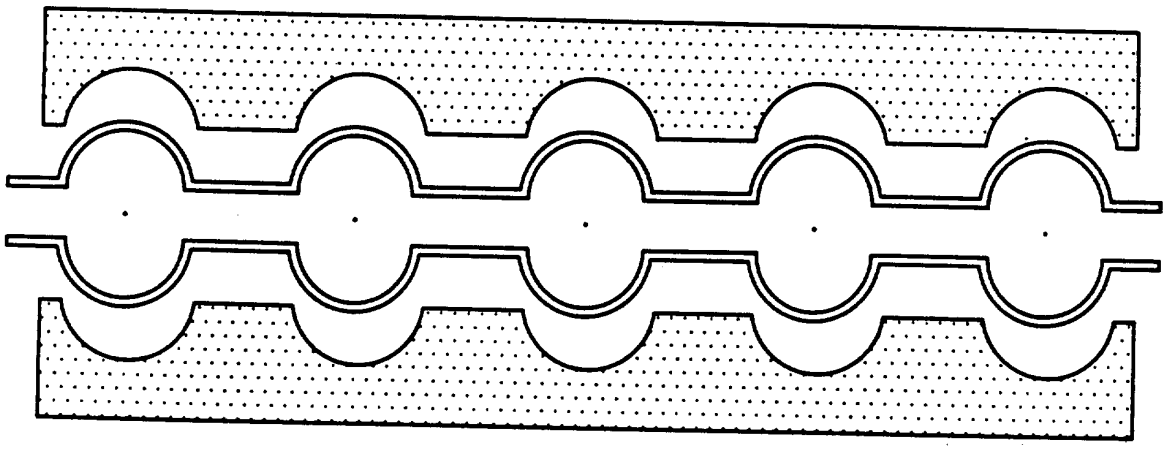

Figure 29

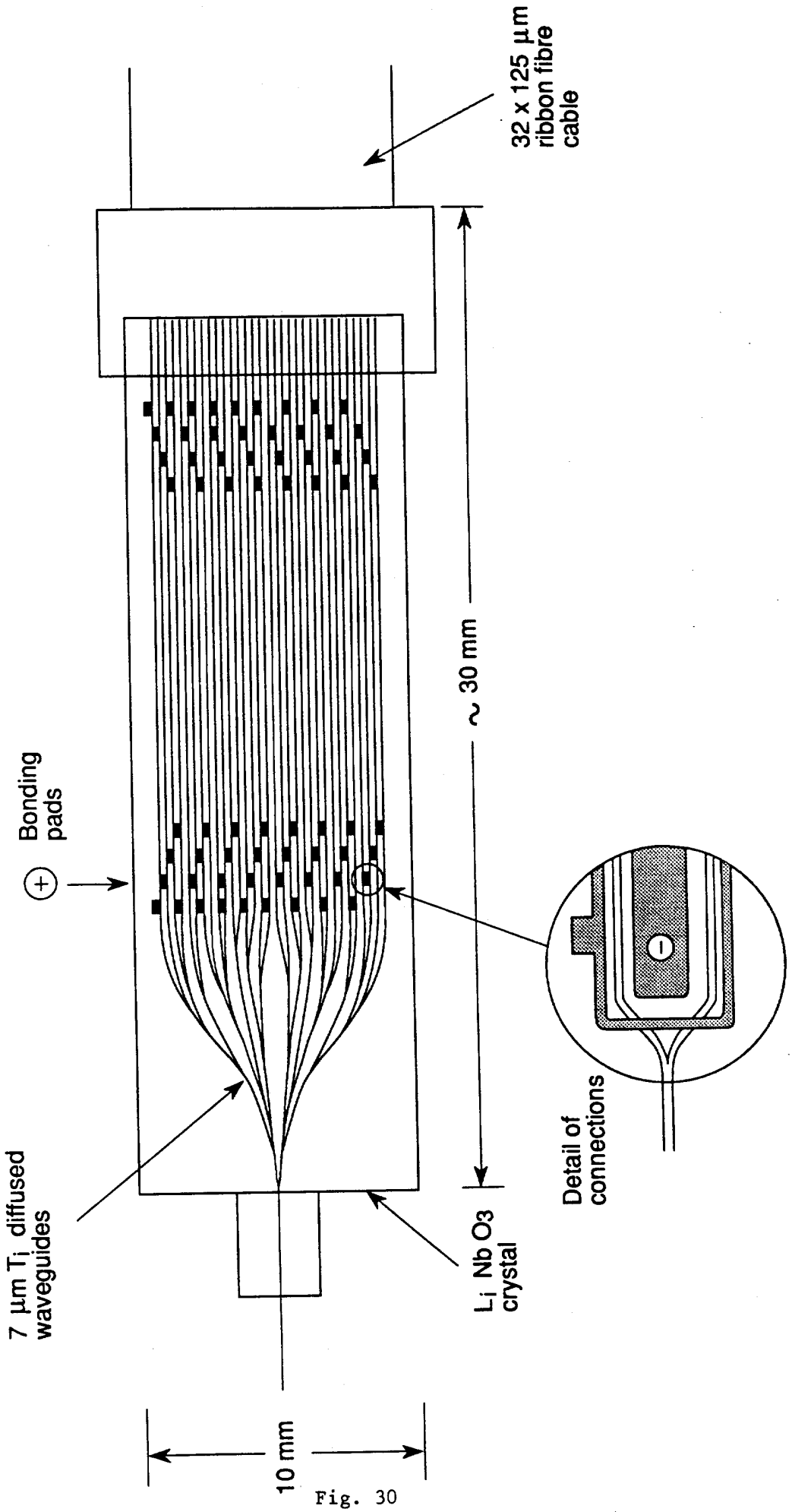

Figure 30

Fig. 30

Imprimé au CERN. Prix : 3.30 Fr.